Thermochronology of the Western Alps (Pelvoux Massif) Reveals the Longterm Multiphase Tectonic History of the European Paleomargin

Louise Boschetti, Frédéric Mouthereau, S. Schwartz, Y. Rolland, M. Bernet, M. Balvay, N. Cogné, Abdeltif Lahfid

Tectonics®

RESEARCH ARTICLE
10.1029/2024TC008498

Thermochronology of the Western Alps (Pelvoux Massif) Reveals the Longterm Multiphase Tectonic History of the European Paleomargin

L. Boschetti[1,2], F. Mouthereau[1], S. Schwartz[2], Y. Rolland[2,3], M. Bernet[2], M. Balvay[2], N. Cogné[4], and A. Lahfid[5]

[1]Géosciences Environnement Toulouse, Université de Toulouse Paul Sabatier, CNRS, IRD, Toulouse, France, [2]ISTerre, Université Grenoble Alpes, USMB, CNRS, IRD, UGE, Grenoble, France, [3]EDYTEM, Université Savoie Mont Blanc, CNRS, UMR 5204, Le Bourget du Lac, France, [4]Géosciences Rennes, Université Rennes 1, UMR, CNRS 6118, Rennes, France, [5]BRGM/ISTO, Orléans, France

Abstract The Variscan and Alpine long-term thermal evolution of the European paleomargin in the external Western Alps is still unknown, although important for reconstructing the geodynamic evolution of this orogen. Here we combine zircon fission track and apatite fission track and U-Pb double dating analyses of the Pelvoux massif in the Western Alps. Apatite U-Pb ages of <310 Ma and >320 Ma define a bimodal age distribution that reflects differential cooling across the East Variscan Shear Zone. QTQt thermal history modeling reveals a two-stage rifting evolution on the European paleomargin, initiated with the Alpine Tethys rifting episode during the Early Jurassic and reactivated during the Cretaceous Valais rifting event, leading to peak temperatures of ~350°C at 90 Ma. The subsequent cooling records a pre-Priabonian phase of exhumation between 80 and 50 Ma that is related to N-S oriented Pyrenean shortening. It is followed by Alpine collision-related burial of the Pelvoux massif from below the foreland basin and the Penninic Frontal Thrust at around 30–25 Ma.

Key Points:

- We present new zircon fission track, zircon fission track, and U-Pb/Apatite data for SW Alps Pelvoux to connect late Variscan to Mesozoic and Alpine Cenozoic thermal history
- This study highlights pre-structuring by the East Variscan Shear Zone
- We identified a major Cretaceous (110–90 Ma) thermal peak caused by Valaisan opening which is followed by N-S shortening

Supporting Information:

Supporting Information may be found in the online version of this article.

Correspondence to:

L. Boschetti,
louise.boschetti@univ-tlse3.fr

Citation:

Boschetti, L., Mouthereau, F., Schwartz, S., Rolland, Y., Bernet, M., Balvay, M., et al. (2025). Thermochronology of the western Alps (Pelvoux massif) reveals the longterm multiphase tectonic history of the European paleomargin. *Tectonics*, *44*, e2024TC008498. https://doi.org/10.1029/2024TC008498

Received 15 JUL 2024
Accepted 23 JAN 2025

Author Contribution:

Supervision: S. Schwartz
Visualization: S. Schwartz
Writing – review & editing: S. Schwartz

1. Introduction

The tectonic structure and thermal properties of rifted margins exert a well-established influence on the temporal and spatial distribution of shortening, exhumation, and thermal evolution of orogenic belts (e.g., Bellahsen et al., 2014; Beltrando et al., 2014; Célini et al., 2023; Jammes & Huismans, 2012; Jourdon et al., 2019; Manatschal et al., 2021; Masini et al., 2012; McIntosh et al., 2013; Mesalles et al., 2014; Mohn et al., 2014; Mouthereau et al., 2013, 2014, 2021; Vacherat et al., 2014). In case of continental margins that have recorded multiple thinning events, identifying the specific effects of a given rift event on collisional evolution can prove challenging. The lithosphere of Western Europe is a good example of multiple rifting events. It was stretched since the Permian-Triassic through the Jurassic and Cretaceous periods, leading to the opening of the Neo-Tethys, Alpine Tethys and Bay of Biscay (e.g., Mouthereau et al., 2021) and in Neogene times, with the opening of the Western Mediterranean Sea (e.g., Boschetti et al., 2023). These Mesozoic rifting events led to the fragmentation of Western Europe into the north Iberia-Ebro and Adria microplates (van Hinsbergen et al., 2020). From the Middle to Late Cretaceous, the convergence of the Iberia-Ebro and Adria microplates relative to Europe, which was initially oblique, became orthogonal, resulting in the Pyrenean and the Alpine collision (van Hinsbergen et al., 2020; Angrand & Mouthereau, 2021). The Alpine arc (Figure 1) is the result of the subduction of the Alpine Tethys, followed by the accretion of the paleomargins of Adria during the Late Cretaceous period (e.g., Handy et al., 2010; Schmid et al., 2004; van Hinsbergen et al., 2020), and of Europe mostly during the Cenozoic (e.g., Dumont et al., 2012, 2022; Lagabrielle et al., 2015; Lanari et al., 2014; Schmid et al., 1996, 2004; Simon-Labric et al., 2009; Wiederkehr et al., 2009). The north-north-west oblique movement of the Adriatic plate relative to the European plate resulted in the inversion of the Variscan basement currently exposed in the Western Alps as the External Crystalline Massifs (ECMs) (Figure 1), which originally formed the hyper-extended and necking domains of the European rifted margin (e.g., Lemoine et al., 1986; Ribes et al., 2019). Seismic tomography data show that the deep root of the collisional wedge is partly underthrusted below the subduction wedge (e.g., Schwartz et al., 2024). Geochronological constraints reveal that this process was associated with the development or reactivation of major shear zones around 34-30 Ma (Cenki-Tok et al., 2014; Gasquet et al., 2010; Leloup et al., 2005; Rolland & Rossi, 2016; Sanchez et al., 2011; Simon-Labric et al., 2009) followed by the exhumation of ECMs since ca. 20 Ma. Exhumation of ECMs results from a combination of frontal thrusting, which propagates in the frontal fold and thrust belt after 16 Ma (Bilau, Bienveignant, et al., 2023; Mai yung Sen et al., 2025) and

10.1029/2024TC008498

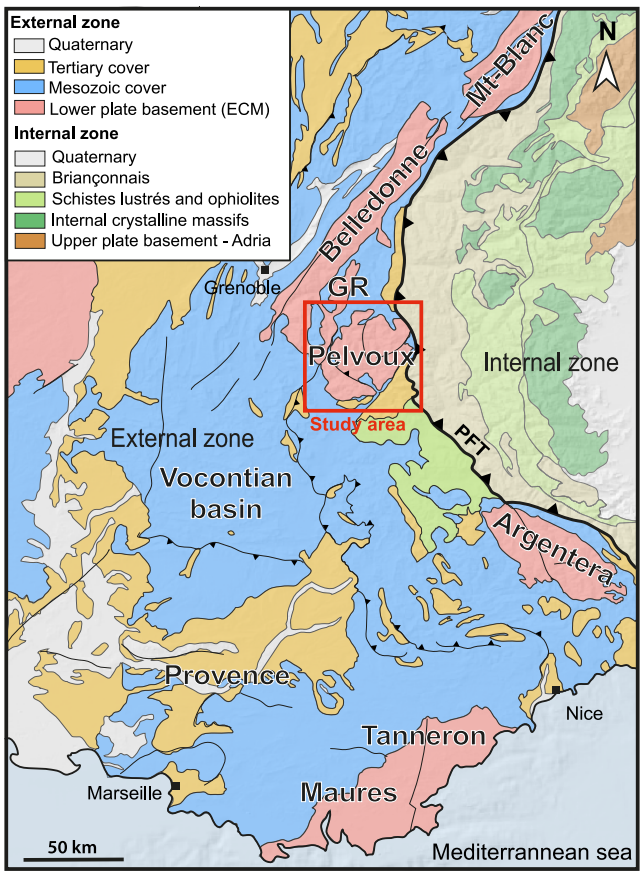

Figure 1. Simplified geological map of the south west Alpine belt. The studied area is identified by a red frame, which correspond to the Pelvoux massif. ECM: External Crystalline Massifs: GR: Grandes Rousses; PFT: Penninic Frontal Thrust.

extensional unroofing along the PFT (Bilau et al., 2021, 2025). This exhumation appears to be diachronous from north to south, with younger zircon fission track (ZFT) thermochronological ages recorded in the Mont Blanc ECM (ZFT ages of 11.5 Ma), and older ages is in the South Belledonne ECM (ZFT ages of 29 Ma) (Fugenschuh & Schmid, 2003; Girault et al., 2022; Glotzbach et al., 2008; Seward & Mancktelow, 1994). Whereas the most recent post-30 Ma collision-related exhumation events of the ECMs are well understood, especially in the Mont-Blanc and Belledonne massifs (e.g., Mercier et al., 2023; Rolland et al., 2009), these existing geochronological and thermochronological constraints fail to resolve the details of the thermal evolution of the European margin during the transition from the Variscan chain, Mesozoic rifting to the Alpine subduction collision. Therefore, it is yet unclear how the pre-Alpine tectonic events have been distributed on the European paleomargin and how they have impacted the architecture and the tectono-thermal evolution of the Western Alps. In the southern part of the Pelvoux and NW part of the Argentera massifs, ZFT ages are more complex and seem to preserve an older Cretaceous thermal event (Beucher et al., 2012; Bigot-Cormier et al., 2000, 2006; Bogdanoff et al., 2000; Seward et al., 1999; van der Beek et al., 2010). Moreover, there is stratigraphic evidence that at least parts of the Pelvoux massif were exhumed to the surface before the Alpine collision. This is illustrated by the pre-Priabonian unconformity at the contact between the Variscan basement and the onlapping Priabonian flyschs (e.g., Dumont et al., 2012). Below the unconformity, EW-directed and south-vergent folds reveal a deformation event that coincided in time and direction with the so-called Late Cretaceous to Eocene "Pyrenean" shortening phase (e.g., Bilau, Rolland, et al., 2023; Ford, 1996; Lazarre, 1997; Sue et al., 1997).

The pre-Alpine ZFT ages observed in the Pelvoux massif indicate a maximum burial temperature of 250°C during the Oligocene collision (Seward et al., 1999). This agrees with studies on fluid inclusions or chlorite thermometry that indicate a maximum Alpine burial temperature of 250°C below the Penninic Frontal Thrust (PFT; Seward et al., 1999; Tricart et al., 2001, 2007; Simon-Labric et al., 2009; Potel & Trullenque, 2012). These ZFT-derived maximum burial temperatures contrast with temperatures of 300–350°C resolved in inverted Jurassic basins of the ECMs using Raman Spectrometry on Carbonaceous Material (RSCM) (Balansa et al., 2022; Bellanger et al., 2015; Célini et al., 2023). These maximum burial temperatures have been interpreted to result from Alpine burial by several authors (Balansa et al., 2022; Bellanger et al., 2015), although they could alternatively be pre-Alpine due to heating (and burial) during the Jurassic and Cretaceous rifting phases, as identified in the Vocontian basin, now structurally inverted in the Digne Nappe (Célini et al., 2023). The lack of more precise constraints on the temperature-time evolution limits our understanding of the timing of pre-Alpine peak temperatures, pre-alpine exhumation, and their related processes. Here, we use new ZFT analyses, for tracing the timing of exhumation of the Pelvoux massif before it was involved in the Alpine deformation. The initial pre-Alpine geometry of the Variscan basement of Europe is also a matter of debate as some authors propose a continuity between the Southern Maures-Tanneron and Sardinia basements (e.g., Carosi et al., 2012; Corsini & Rolland, 2009; Simonetti, Carosi, Montomoli, Corsini, et al., 2020; Simonetti, Carosi, Montomoli, Cottle, & Law, 2020), or significant post Variscan lateral displacements and rotations (e.g., Edel et al., 2018). To connect this history with a pre-Mesozoic post-Variscan temperature evolution in comparison to the Maures-Tanneron massif and the younger Alpine Cenozoic exhumation event we also carried out apatite fission track (AFT) and U-Pb double dating analyses on crystalline rocks of the Pelvoux massif. Inverse modeling of thermochronological data was then undertaken to reconstruct the thermal history.

2. Geological Setting

The basement of the Pelvoux massif consists of different metamorphic and igneous rocks (Figure 2a), including gneisses, amphibolites, migmatites, and anatectic granites of Precambrian to Carboniferous age that were

10.1029/2024TC008498

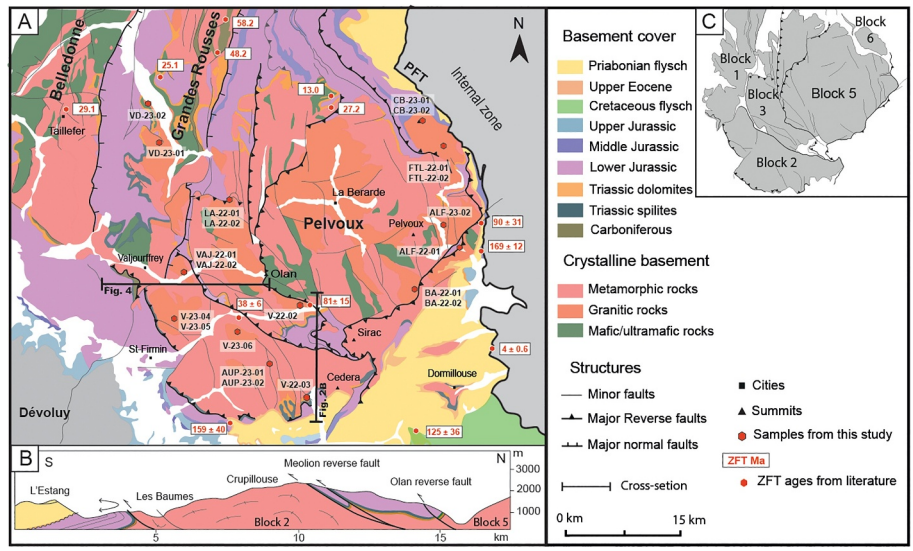

Figure 2. (a) Geological map of the Pelvoux Massif with the location of dated samples. Previous ZFT data are from Seward et al. (1999), van der Beek et al. (2010), and Girault et al. (2022). (b) North-south geological cross-section with depicting the north-south pre-Priabonian shortening. (c) Position of major structural blocks (blocks 1, 2, 3, 4, 5, and 6).

deformed and metamorphosed during the Variscan orogeny (Fréville et al., 2022; Guillot et al., 2009; Jacob et al., 2022). Permian sediments and magmatic rocks are not present in the Pelvoux massif, a feature that is shared by the majority of the ECMs (e.g., Ballèvre et al., 2018). The Mesozoic sediments rest upon the crystalline basement, with an erosional surface that is related to the dismantling of the Variscan chain during Permian to Triassic times (e.g., Barféty, 1985). The Pelvoux massif can be structurally divided into several blocks bounded by major faults (Figures 2b and 2c). These major faults were involved first during the Variscan cycle and then during the Jurassic rifting and compressional tectonic inversion that affected the European margin (e.g., Schwartz et al., 2024). North-South segmentation was first developed during the late stages of the Variscan orogeny, along the East Variscan Shear Zone (EVSZ, Carosi et al., 2012; Corsini & Rolland, 2009; Guillot et al., 2009; Simonetti, Carosi, Montomoli, Carosi, et al., 2020; Simonetti, Carosi, Montomoli, Cottle, & Law, 2020). Block 1 is delimited by the Bourg d'Oisans Jurassic normal fault in the east, the Grandes Rousses massif in the north and the Valjouffrey valley in the south. The southern block 2 is bounded by a major south-vergent thrust where the basement overrides the Liassic sediments. Block 2 is separated from block 3 by the "Aiguille de Morge" reverse fault. Block 3 is delimited to the north by the Olan reverse fault, which is the southern boundary to block 5. The blocks 4 and 5 are separated by the "La Grave" and "Saint Christophe" reverse faults. Finally, block 6, which is the closest to the PFT, is separated from block 5 by the Combeynot reverse fault.

The onset of the Alpine cycle is argued by marine incursion and deposition of Late Triassic dolostones associated with basaltic flows ("spilites'; Laurent, 1992). The syn-rift extension leading to Alpine Tethys opening is shown by the development of fault bounded basins filled with Early and Middle Jurassic shallow to deep-marine sediments (Barféty, 1985; Lemoine et al., 1986). Then, two different compressive phases affected the massif. The first one is related to the Cretaceous-to-Eocene pre-Alpine Pyrenean-Provence phase of deformation. This deformation corresponds to a north-south shortening, leading to east-west-trending, south-verging folds in the Pelvoux massif. The second one corresponds to the Late Eocene-Early Oligocene Alpine phase marked by the deposition of "Grès du Champsaur" flysch (Figure 2b) (Dumont et al., 2008; Ford, 1996; Lazarre, 1997; Sue et al., 1997). The Alpine phase is associated with north-west south-east oriented shortening (e.g., Ford & Lickorish, 2004), as the PFT propagated toward the foreland (Dumont et al., 2008, 2012). During this phase, the Pelvoux massif was partially tectonically buried under the PFT from 34 to 31 Ma (Bellanger et al., 2015; Ceriani et al., 2001; Simon-Labric et al., 2009), and shows reactivation of east-west faults in a strike-slip mode within the massif (Simon-Labric et al., 2009), whereas the north-south faults show compressional reactivation. The metamorphism related to this burial phase did not exceed the greenschist facies conditions (280°C, Simon-Labric et al., 2009). The last stage of exhumation is documented by AFT and (U-Th)/He analyses showing cooling below 200°C between 28 and 5 Ma (Beucher et al., 2012; Seward et al., 1999; Van der Beek et al., 2010). The

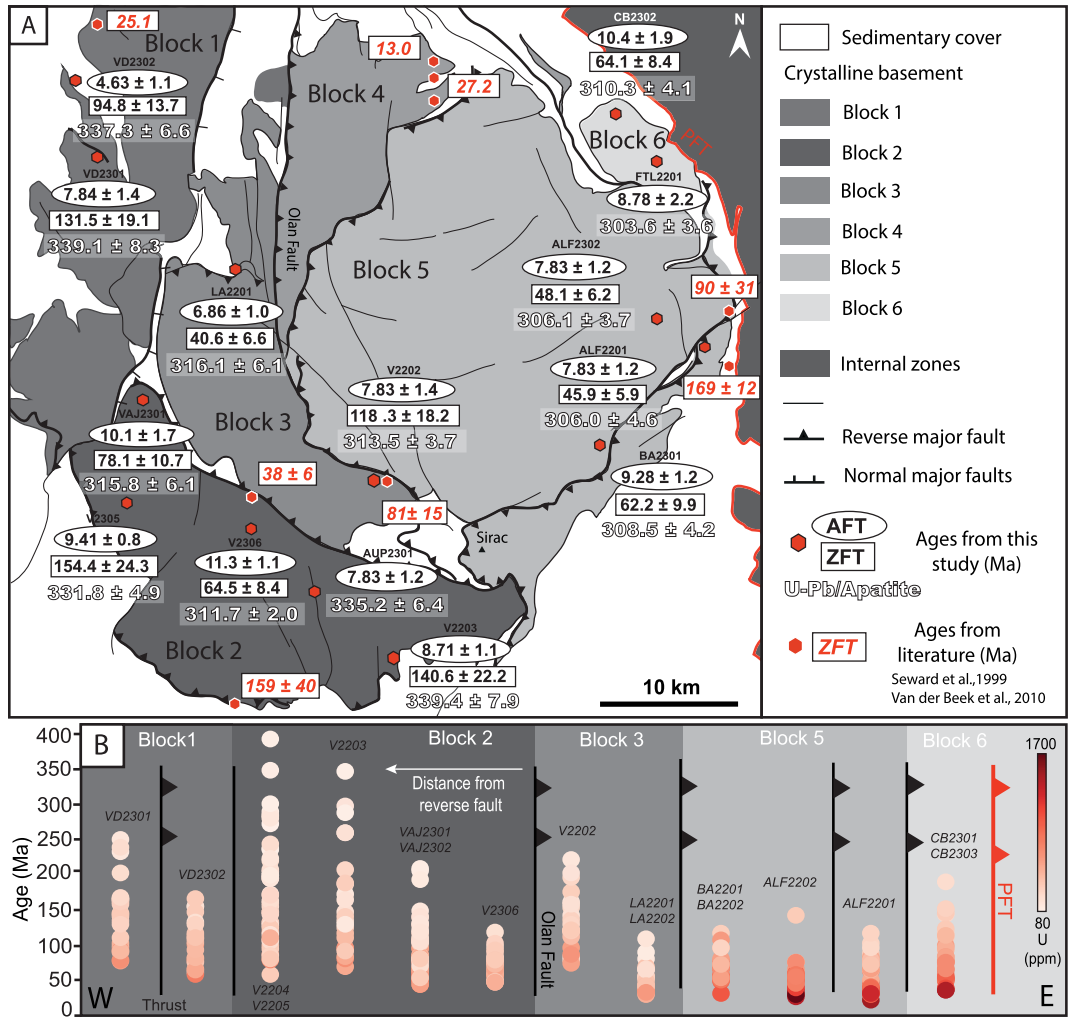

Figure 3. (a) Structural map of the Pelvoux massif depicting low-temperature thermochronological ages obtained from this study and ages from the literature. (b) Synthetic east-west showing for each sample the individual ZFT grain ages together with their uranium content in each tectonic block.

low-temperature metamorphic conditions associated with the formation of the collisional prism precluded a uniform thermal resetting of low-temperature thermochronometers at the scale of the massif. In the northern central part of the Pelvoux massif (Meije zone in Figures 2a and 3) show full resetting of ZFT and AFT ages with clear Alpine cooling ages ranging from 13.7 ± 1.6 to 3.2 ± 0.4 Ma (van der Beek et al., 2010). In the southern part of the massif, however, ZFT apparent cooling ages are partially reset or unreset, as indicated by mixed pre-Alpine ZFT ages ranging from 81 ± 15 to 38 ± 6 Ma to (Figures 2a and 3) (Seward et al., 1999). Interestingly, the RSCM derived temperatures estimates show a uniform distribution of the maximum burial temperature of Jurassic sedimentary strata, ranging from 250 to 300°C across the massif and its peripheral basins (Balansa et al., 2022; Bellanger et al., 2015; Célini et al., 2023), whereas the pattern of partially reset and unreset ZFT low-temperature cooling ages indicate that maximum burial temperatures may be less than 250°C in some parts of the massif during the Alpine orogeny and RSCM temperatures could therefore be inherited from former pre-alpine thermal events.

3. Methods

3.1. Sampling Strategy and Sample Preparation

Twenty samples were collected from granitoids of the Pelvoux massif (Figure 2a; Table 1). To account for variable zircon and apatite fertility we selected two rock samples from slightly different lithologies in each

Tectonics

10.1029/2024TC008498

Table 1

Localization Fission Track and U-Pb Data (Boschetti, 2024, https://doi.org/10.18709/PERSCIDO.2024.07.DS410)

Sample	Lat	Long	Mnx	Central age (Ma)	2s	Ns	Ni	Sq no./Area (cm^2)	Grain no.	Disp (%)	p(chi^2)	RhoS	RhoI	U (ppm)	2s	Dpar (μm)	MTL (μm)	U-Pb (Ma)	2s
FTL2302	45.00383	6.43799	Zr	–	–	–	–	–	–	–	–	–	–	–	–	–	–	–	–
			Ap	8.8	2.2	136		1.14E − 03	31	18.5	12.8	–	–	–	–	1.4	14.5	303.2	3.6
LA2201	44.93929	6.1435	Zr	38.9	8.6	317	131	83	7	8.78	0.07	6.0E + 06	2.47E + 06	436	77	–	–	–	–
			Ap	6.9	1.0	196	–	1.30E − 03	39	0	0.24	–	–	–	–	1.7	13.4	316.1	6.1
LA2202	44.93929	6.1435	Zr	40.6	6.6	730	291	191	18	16.9	15.7	6.0E + 06	2.38E + 06	419	50	–	–	–	–
			Ap	–	–	–	–	–	–	–	–	–	–	–	–	–	–	–	–
VD2301	45.00984	6.03943	Zr	131.5	22.3	2,475	310	243	23	22.4	2.4	1.6E + 07	2.00E + 06	342	40	–	–	–	–
			Ap	7.9	1.4	133	–	2.19E − 03	40	0	0.87	–	–	–	–	63.5	–	339.1	8.3
VD2302	45.03972	6.03355	Zr	94.8	13.7	1,883	329	203	21	17.1	7.7	1.5E + 07	2.54E + 06	434	49	–	–	–	–
			Ap	4.6	0.9	98	–	1.66E − 03	38	0	1					53.9		337.3	6.6
ALF2201	44.87746	6.47678	Zr	45.9	7.6	1,709	604	184	25	27.3	0	1.5E + 07	5.14E + 06	900	77	–	–	–	–
			Ap	8.5	1.2	187	–	1.45E − 03	40	0	0.9	–	–	–	–	66.6	–	306	4.6
ALF2302	44.89145	6.44758	Zr	48.1	9.7	1,617	548	219	28	41.9	0	1.2E + 07	3.92E + 06	684	61	–	–	–	–
			Ap	8.8	1.8	157	–	1.35E − 03	35	23.16	0.32	–	–	–	–	55.9	–	306.1	3.7
AUP2301	44.77523	6.19448	Zr	217.7	47.0	1,352	102	140	9	14.2	30.04	1.5E + 07	1.14E + 06	194	39	–	–	–	–
			Ap	11.6	1.1	445	–	1.60E − 03	38	0	0.75	–	–	–	–	2.2	13.9	335.2	6.4
BA2201	44.83265	6.39421	Zr	60.3	9.2	1,134	307	106	15	0.5	83.2	1.7E + 07	4.53E + 06	789	92	–	–	–	–
			Ap	9.3	1.2	240	–	1.58E − 03	38	1.2	0.96	–	–	–	–	1.8	15.2	308.5	4.2
BA2202	44.83299	6.39151	Zr	68.6	24.4	483	115	56	7	41.8	0.1	1.4E + 07	3.21E + 06	557	105	–	–	–	–
			Ap	–	–	–	–	–	–	–	–	–	–	–	–	–	–	–	–
CB2301	45.01221	6.41086	Zr	99.7	26.8	850	142	88	10	30.3	1	1.5E + 07	2.53E + 06	429	73	–	–	–	–
			Ap	9.2	2.0	95	–	1.07E − 03	27	0	0.78	–	–			–	–	304.8	4.1
CB2303	45.01834	6.41365	Zr	64.1	11.8	1,860	487	166	23	33.3	0	1.8E + 07	4.59E + 06	777	73	–	–	310.3	4.1
			Ap	10.4	1.9	117	–	1.53E − 03	37	1.93	0.64	–	–	–	–	–	–	313.5	3.7
V2202	44.82678	6.24263	Zr	125.5	18.2	1,894	237	211	21	7.5	40.9	1.4E + 07	1.76E + 06	316	42	–	–	–	–
			Ap	7.8	1.4	157	–	1.60E − 03	40	17.14	0.65	–	–	–	–	1.83	14.4	339.5	7.9
V2203	44.73097	6.24607	Zr	140.6	27.8	2,169	243	233	23	29	0.6	1.5E + 07	1.63E + 06	292	39	–	–	–	–
			Ap	8.7	1.1	252	–	1.51E − 03	37	0	0.48					2.4	14.1	331.8	4.9
V2204	44.82164	6.0672	Zr	152.3	32.2	1,824	189	211	20	28.5	1.1	1.4E + 07	1.40E + 06	250	37	–	–	–	–
			Ap	9.4	0.8	552	–	1.66E − 03	40	2.87	0.21	–	–	–	–	1.4	12.3	321.4	4.7
V2205	44.82164	6.0672	Zr	161.9	21.4	2,117	207	259	24	26.6	2.5	1.3E + 07	1.25E + 06	222	32	–	–	–	–
			Ap	10.7	1.2	321	–	1.42E − 03	39	0	1.16	–	–	–	–	1.7	12.8	311.7	2
V2206	44.80341	6.16386	Zr	64.5	8.4	2,077	516	342	27	2.9	25.8	9.5E + 06	2.36E + 06	418	39	–	–	–	–
			Ap	11.3	1.1	516	–	1.34E − 03	40	8.12	0.27	–	–	–	–	1.5	14.0	315.8	6.1
VAJ2301	44.8695	6.0823	Zr	67.8	8.1	2,784	675	300	31	15.5	5.2	1.5E + 07	3.52E + 06	405	49	–	–	–	–
			Ap	10.0	1.7	136	–	1.87E − 03	38	0	0.58	–	–	–	–	1.6	13.3	–	–
VAJ2302	44.8695	6.0823	Zr	105.7	21.4	1,819	283	188	20	32.6	0	1.5E + 07	2.36E + 06	–	–	–	–	–	–

tectonic block. Samples were prepared at the ISTerre Geo-ThermoChronology (GTC) platform, Université Grenoble Alpes, France. The 160–80 μm fraction was separated with standard magnetic and heavy liquid separation techniques. Eighteen samples yielded sufficient zircons for fission track analysis and 16 were selected for AFT analysis and apatite U-Pb geochronology.

3.2. Zircon Fission Track Dating

ZFT analyses were done at the ISTerre GTC fission-track laboratory. Zircon aliquots were mounted in Teflon® sheets, polished and etched between 13 and 41 hr in a NaOH-KOH melt at 228°C in a laboratory oven. Then, Teflon® mounts were covered with muscovite sheets as external detectors and irradiated at the Oregon State University together with IRMM541 (50 ppm U) dosimeter glasses and Fish Canyon Tuff age standards (Naeser et al., 1981). After irradiation, the mica detectors were etched at 20°C for 18 min in 48% hydrofluoric acid revealing induced fission-tracks. Samples were analyzed and fission tracks were counted using an Olympus BX51 optical microscope at 1250x magnification with the FTStage 4.04 system (Dumitru, 1993). The Zeta factor calibration (Hurford & Green, 1983) was employed to determine the individual fission track ages.

3.3. Apatite Fission Track and U-Pb Double Dating

All AFT analyses were performed at the GeOHeLiS platform, University of Rennes, France. FT and U-Pb data were acquired simultaneously during laser ablation, using an ESI NWR193UC Excimer laser coupled to an Agilent 7700x Q-ICP-MS. We employed an energy of 3.9 J/cm^2 and a repetition rate of 5 Hz with a 40 mm round spot. Analytical details are provided in Supporting Information S1. Prior to LA-ICP-MS analysis, track etching was performed with a 5.5 M HNO_3 at 21°C for 20s. The grain mounting and etching are similar to the protocol described by Donelick et al. (2005). Spontaneous fission track counting was carried out using a Zeiss Axio Imager M1 equipped with an automated stage system using the TrackWorks software at a magnification of 1000x. Dpar values were measured to be used as kinetic indicators in the subsequent inverse modeling (see Section 3.4). The FT dating used the ζ protocol of Cogné et al. (2020). ICP-MS machine drift was corrected using the artificial glass NIST 612 (Jochum et al., 2011) and Durango apatite shards (McDowell et al., 2005) analyzed during a primary session were revisited to calculate the fractionation factor. The age calculation was implemented using an in-house python script and produced single grain ages as well as both central (Galbraith & Laslett, 1993) and pooled ages, P(χ2) and age dispersion for the dated sample. The same script produced the radial plots (Galbraith, 1990). The Madagascar apatite (Thomson et al., 2012) was used as primary standard to calculate U-Pb ratios. An in-house python script was used for U-Pb age calculation and Tera-Wasserburg plots. The best fit regression line (and its uncertainty envelope) for the population of $^{207}Pb/^{206}Pb$ and $^{238}U/^{206}Pb$ ratios was calculated with the York et al. (2004) algorithm. The lower intercept of this line with the Concordia in the Tera-Wasserburg space (and its uncertainty) was calculated using the approach of Ludwig (1980). McClure Mountain apatite (Schoene & Bowring, 2006) was used as secondary standards for both U-Pb and AFT dating (Cogné et al., 2024). Durango apatite used for the ζ protocol was also used as secondary quality control material for U-Pb dating. Fish Canyon Tuff apatites (Gleadow et al., 2015) were also dated for AFT during the first analytical session.

3.4. Thermal History Modeling

To constraint the thermal history of the rocks sampled, we performed inverse modeling of ZFT and AFT data using the version v5.8.0 of the QTQt software (Gallagher, 2012). The inversion procedure uses a Bayesian "Markov chain Monte Carlo" (MCMC) algorithm to determine the best time-temperature path that reproduces our data through a large number, in our case about 300,000 on average, comprising burn-in and postburn-in, of MCMC tested solutions. This implies that a model is generated by modifying a parameter of the existing model for each novel solution. Apatite U-Pb ages were incorporated as prior parameter in the model as a first box constraint, with 320 ± 10 Ma from our data and 450°C ± 50 (Kirkland et al., 2018) to start the sample path. As an output, QTQt proposed several temperature-time paths: (a) the "Max Likelihood model," which most closely reproduces the data but is highly complex, (b) the "Max Posterior model", which is a simpler model and a better fit to a coherent geological history, but fits the data less well, (c) the "Max Mode Model", which represents the probability peaks in 1D over the entire distribution of the model produced and, finally, (d) the "Expected model", which is the preferred single model in which all previous models are considered. QTQt incorporates kinetic models for diffusion in apatite crystals that account for radiation damage production and annealing. The AFT

multi-kinetic annealing model of Ketcham et al. (2007) was used to invert the AFT data (ages and lengths) using Dpar as kinetic indicator. For ZFT, the data annealing model of Tagami et al. (1998) and Yamada et al. (2007) was applied for crystalline zircons very low amount of accumulated radiation. The closure temperature for these zircons is estimated to be about 340°C (Rahn et al., 2004; Reiners & Brandon, 2006). The temperature required for a total or partial annealing of fission tracks in zircon depends on the hold time at given temperature and the amount of accumulated radiation damage, which is influenced by the uranium concentration of the zircon. For naturally damaged zircons the temperature of the zircon partial annealing zone is about 238–180°C for a 10 Myr hold time within this temperature range (Brandon et al., 1998; Reiners & Brandon, 2006). The Pelvoux massif grains are variably metamict due to a large amount of accumulated radiation damages and QTQt does not provide a suitable annealing model for this type of grain. Nonetheless, we choose to adopt the annealing model of Tagami et al. (1998) and treated our results with caution as the modeled maximum temperature may be overestimated. Two time-temperature constraint boxes were chosen based on geological data. These constraint boxes are assumed to represent: (a) the surface temperature conditions (10 ± 10°C) achieved during deposition of Triassic to Jurassic (Toarcian) continental to shallow marine units that were deposited on the Variscan basement (Barfety et al., 1970; Barféty & Gidon, 1983; Lemoine et al., 1986; Roux et al., 1988; Rudkiewicz, 1988) and (b) the Priabonian, when the Champsaur flysch were deposited on the Pelvoux crystalline basement at 37 ± 2 Ma. Geological structures define different tectonic blocks in the massif, and thus potential different thermal histories. Therefore, each block was modeled separately.

4. Results

4.1. Apatite U-Pb Data

598 U-Pb analyses were performed on apatite grains obtained from 16 samples with an average number of grains of 37 grains per sample (Table 1; Figure S1 in Supporting Information S1). They show lower intercept age in the Tera-Wasserburg diagram ranging from 339.1 ± 7.5 to 303.2 ± 3.6 Ma (Figures 1 and 3, Table 1). An east-west trend can be observed in the distribution of U-Pb ages: (a) older samples in the western blocks (blocks 1 and 2), with U-Pb ages greater than 330 Ma and an average of 338.2 ± 7.5 Ma for block 1 and 326.8 ± 5.5 Ma for block 2, (b) intermediate U-Pb ages in block 3 with mean age of 314.5 ± 4.9 Ma and (c) the youngest ages in the eastern blocks (block 5 and 6) with ages <310 Ma and a mean age of 306.7 ± 4.2 Ma for block 5 and 306.9 ± 3.8 Ma for block 6 (Figure 3a).

4.2. Apatite Fission Track Data

Central ages range from 11.57 ± 1.1 to 4.63 ± 0.93 Ma (Table 1; Figure S2 in Supporting Information S1) and all of them show a $p(\chi^2) > 0.05$ denoting a likely single age population per sample (Galbraith, 2005). Sample CB2301 contains 5 grains with very low U contents that have not been considered for age calculation. Only few track lengths could be measured due to the young ages and thus low track density. All but one is >13.5 µm, denoting a relatively fast cooling through the Partial Annealing Zone (PAZ, define between 120 and 60°C, Gallagher et al., 1998). Dpar values are mostly <2 µm except for V22-3 and AUP23-1, denoting fast annealing flour apatites (Donelick et al., 2005). An age-elevation plot reveals a faint trend across the massif, with older ages at higher elevations (Figure S3 in Supporting Information S1).

4.3. Zircon Fission Track Data

ZFT analyses were performed on 18 samples with central ages ranging from to 158.5 ± 31.35 to 38.9 ± 8.65 Ma. 14 samples (LA2202, VD2301, VD2302, ALF2201, ALF2302, BA2201, CB2303, V2202, 2203, V2204, V2205, V2206, VAJ2301, VAJ2302) yield between 18 and 31 grains per sample (Table 1; Figures 3a and 3b; Figure S4 in Supporting Information S1). Four samples containing between 7 and 10 grains (LA2201, BA2202, CB2301, AUP2301) did not yield sufficiently constrained ages and were further considered in this study. In block 1, central ages are around 131.5 ± 19.1 Ma in the hanging wall of the Villard-Notre-Dame fault and of 98.8 ± 13.7 Ma in the footwall part. This younging trend toward the thrust contacts of the adjacent block is observed in each block. In block 2 ages range between 154.4 ± 24.3 and 64.5 ± 8.5 Ma, with ages getting younger in the hanging wall toward the east when approaching block 3 (Figure 4). We observe the same trend in block 3 and block 5, with ages ranging from 118.3 ± 18.2 to 40.6 ± 6.6 Ma and ages from 62.2 ± 9.9 to 48.1 ± 6.2 Ma, respectively. We note that in block 5, ZFT ages are distinctively younger than in the other blocks.

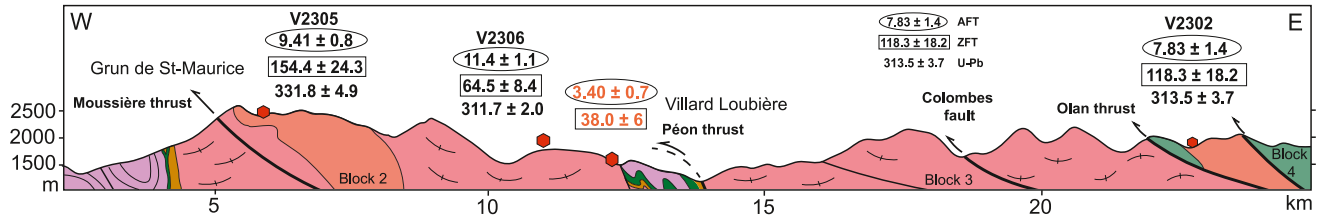

Figure 4. E-W directed geological cross section of the Pelvoux massif and low-temperature thermochronological ages from this study (see location and legend on Figure 2A). Ages in red are from Seward et al. (1999).

4.4. Thermal History Modeling

Block 1 is represented by granite samples VD2301 and VD2302 (Figures 3a and 5a). Model results show that block 1 recorded an initial cooling stage from temperatures compatible with granite formation at 340 Ma to surface temperatures at 200 Ma as the Triassic strata were deposited on top of the granite. Despite some thermal paths indicating burial/tectonic heating during the Mesozoic, the most likely paths remain close to surface temperature. This period lasted until the heating to temperature of 300°C following the deposition of the Priabonian flysch and PFT activation (Figure 5a). Final cooling to the surface occurred around 30 Ma (Figure 5a). The complexity of the trajectories calculated during the Mesozoic reflects the annealing behavior of the different zircon populations, whose apparent cooling ages are nevertheless correctly reproduced by the model (Figure S5 in Supporting Information S1). The same applies to the following blocks.

Block 2 is represented by granite samples V2304, V2305, V2203, VAJ2301, VAJ2302, and V2306 (Figures 3a and 5a). Computed thermal paths show that this block recorded a maximum mean temperature of approximately 300°C at around 110 Ma. This thermal peak is followed by cooling from the middle Cretaceous to the Priabonian. The second rapid heating event to temperatures up to 200°C followed the deposition of the Priabonian flysch, and final cooling occurred at 30 Ma.

Block 3, defined by samples V2202 and LA2202 (Figures 3a and 5c), exhibits thermal paths similar to block 2 but with a first heating stage reaching slightly higher temperatures of ∼350°C at 90 Ma, followed by cooling from the Late Cretaceous until the Priabonian. The second heating event after the Priabonian shows maximum temperatures of approximatively 200°C, reached at 20 Ma and followed by rapid cooling to surface temperatures (∼9.5°C/Ma).

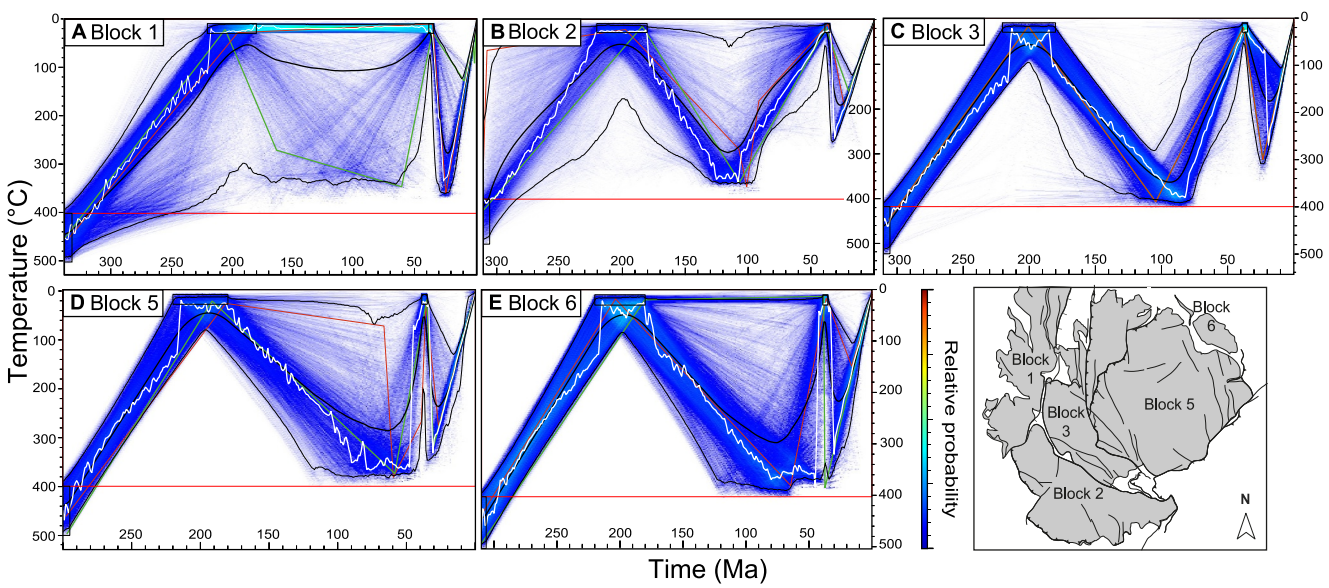

Figure 5. Thermal histories reconstructed for the Pelvoux massif. Results are show for each studied tectonic block (A to D; see location in the insert). Red line: Max Likelihood model; Green Line: Max Posterior model; Black line: Expected model; White line: Max Mode Model. Comparison of predicted and observed AFT and ZFT ages is shown in Figure S3 in Supporting Information S1.

The block 5 thermal history represent granite samples BA2201, BA2202, ALF2201 and ALF2302 (Figures 3a and 5d). After the Triassic, most of the computed paths reveal slow heating up to 300°C during the Jurassic and Cretaceous until cooling occurred at ~80 Ma. After deposition of the Priabonian flysch, a second heating phase reveal that granite of block 5 reached temperature of ~220°C at 30 Ma.

The easternmost block 6 thermal modeling of granite samples CB2301 and CB2303 (Figures 3 and 5e), shows a mixed pattern of thermal paths, not well constrained due to variable sensitivity of ZFT to temperature depending on the variability of accumulated radiation. It includes paths that suggest the sampled rocks remained at surface temperature during the Jurassic-Cretaceous, and those that indicate heating up to 300°C around 75 Ma. The heating phase is followed by a rapid cooling (7.25°C/Ma) until surface temperatures at 35 Ma and a second heating phase up to approximatively 220°C and final cooling starting at 30 Ma, in agreement with results from other blocks.

In summary, inverse modeling resolves a well-constrained Cenozoic heating phase in each block between 30 and 20 Ma to temperatures ranging between 200 and 350°C. The first Jurassic-Cretaceous heating event is less well constrained due to less understood ZFT annealing. The good reproducibility of observed ZFT ages by our inverse thermal models (Figure S5 in Supporting Information S1) reveals the annealing parameters used in our study are well adapted and lead to geologically meaningful results. We note that the higher the temperature reached during the second Cenozoic heating event, the greater the probability of having paths remaining close to surface temperature during the first thermal event. This is particularly well depicted when the temperature of the second heating stage is above 300°C, temperatures associated with the first heating stage are close to surface temperatures, indicating enhanced annealing of fission tracks during the latest thermal event (Figure 3b). On the other hand, if temperatures are below 200°C during the second heating phase, the thermal paths are generally better constrained during the Mesozoic phase of heating. Higher temperatures reached during the second heating stage also result in younger observed (Figure 3b) and predicted ages from 100 to 70 Ma (Figure 5).

5. Discussion

5.1. Late Paleozoic History of the Pelvoux Massif as Inferred From U-Pb Apatite Ages

Our apatite U-Pb ages range between 300 and 340 Ma (Table 1 and Figure 3a). They agree with zircon UPb ages in gneiss and granites of the Pelvoux massif, that are interpreted as metamorphic ages according to the dated thermal peak of Variscan collisional decompression metamorphism estimated at 800–870°C between 337 and 294 Ma (Fréville et al., 2022; Jacob et al., 2022). Apatite U-Pb ages could also reflect thermal resetting associated with upper amphibolite facies conditions related to cooling and decompression stages following the thermal peak. The trend of apatite U-Pb ages, with ages >320 Ma in the western blocks and <310 Ma for the eastern blocks agrees with a major Variscan structure related to a N-S vertical strike-slip shear zone corresponding to the Olan fault (Figure 3a). A similar segmentation is observed on both sides of the Grimaud fault in the Maures-Tanneron massif, where it is interpreted as a differential exhumation of rigid blocks (Morillon et al., 2000). This segmentation is highlighted by amphibole and mica $^{40}Ar/^{39}Ar$ ages corresponding to a temperature range of 350–600°C, somehow similar to that of apatite U-Pb (375–600°C, Kirkland et al., 2018). The western compartment of the Grimaud fault in the Maures massif is characterized by similar amphibole $^{40}Ar/^{39}Ar$ ages as our obtained apatite U-Pb ages in the western Pelvoux blocks, with ages ranging from 329.9 ± 2.1 to 328.1 ± 1.2 Ma. A similar cooling history occurs in the eastern in Maures massif as in the eastern Pelvoux blocks, with amphibole $^{40}Ar/^{39}Ar$ ages of 317.4 ± 2.4 to 307.9 ± 1.2 Ma, in the range of the obtained apatite U-Pb ages. In the Maures massif, this difference in amphibole $^{40}Ar/^{39}Ar$ ages on both sides of the Grimaud fault is interpreted as distinct cooling events between 330 and 300 Ma along this major Variscan fault, which acted as a transtensional to transpressional boundary to the Variscan belt (Gremmel et al., 2023; Rolland et al., 2009). This scenario is supported by monazite geochronology of the Cavalaire fault, which is the southern prolongation of the Grimaud fault (Simonetti, Carosi, Montomoli, Corsini, et al., 2020; Simonetti, Carosi, Montomoli, Cottle, & Law, 2020) and of the Posada-Asinara and Porto Vecchio shear zone in Corsica-Sardinia (Carosi et al., 2012; Giacomini et al., 2008). The Ferriere-Moliere shear zone (FMSZ) in the Argentera massif (Figure 6) is also regarded as a transpressive shear zone active at 340 Ma under amphibolite facies conditions (Carosi et al., 2016; Simonetti et al., 2018). This fault system stretching between Argentera and Maures-Tanneron massifs, is regarded as an anastomosing component of the East Variscan Shear Zone (EVSZ) (e.g., Simonetti, Carosi, Montomoli, Corsini, et al., 2020; Simonetti, Carosi, Montomoli, Cottle, & Law, 2020; Simonetti et al., 2023). This study shows that the Eastern part of the Pelvoux massif exhibits the same trend of exhumation rate as the internal Maures-Tanneron massif during the same period

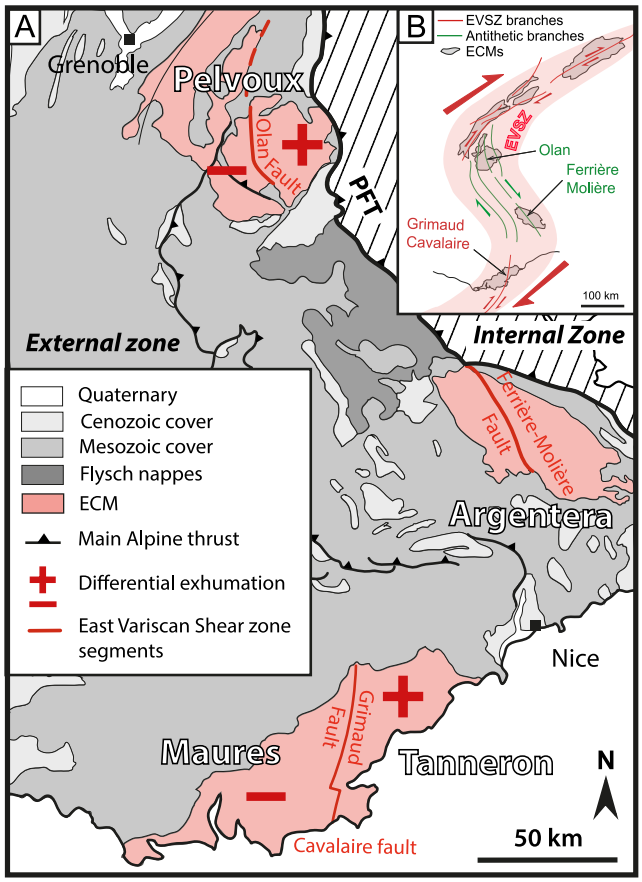

Figure 6. (a) Map of south Alpine External Crystalline Massifs showing the three considered EVSZ branches. (b) The proposed position of the East Variscan shear zone at larger scale, considering paleogeographical reconstruction of Ferriere et al. (2022) for the northern ECMs.

(Figure 6). Furthermore, Freville et al. (2022) demonstrate that the exhumation of the Pelvoux follows a transpressive regime from 325 to 306 Ma, which is also related to the activity of the anastomosed branch of the EVSZ. In this context, the present-day Olan (Pelvoux) and Grimaux/Cavalaire (Maures-Tanneron) faults are considered to belong to two branches of the EVSZ. Moreover, the recent paleomagnetic data (Brunsmann, 2023), imply that the European basement (Pelvoux, Argentera, Maures-Tanneron) has not undergone significant counterclockwise rotation since Permian times. Consequently, the present position and orientation of the Olan, the Ferriere-Molière and the Grimaud/Cavalaire faults can be interpreted as inherited from the late Variscan tectonics along an anastomosed fault system comprising two antithetic branches associated to EVSZ (Figure 6). The Variscan exhumation follows that the cooling path from 300 Ma to the onset of Jurassic rifting at the Triassic-Jurassic transition corresponds to post-Variscan metamorphism cooling related to the dismantling of the Variscan orogen mainly during Permian times (e.g., Vai, 2003).

5.2. Time-Temperature Evolution of the Pelvoux Massif

5.2.1. Pre- "Alpine" Evolution of the Massif

Our thermal models predict that the Pelvoux massif recorded a protracted period of heating from the Early Jurassic toward the end of the Early Cretaceous, followed by cooling between 110 and 70 Ma (Figure 7). This result indicates that the duration of heating, which is commonly associated to rift-related burial and subsidence during the Early Jurassic (e.g., Barféty, 1985; Mohn et al., 2012) and is widely expressed in the field by tilted blocks of the European margin (Lemoine et al., 1986; Figure 7), lasted longer than previously thought.

The Pelvoux massif is regarded as having recorded several kilometers of burial beneath deep-sea sediments (e.g., Barféty, 1985; Manatschal et al., 2021; Mohn et al., 2012). Célini et al. (2023) also placed the Pelvoux massif in the necking domain of the European margin at the transition to the hyper-extended or oceanic domains of the Valaisan basin to the East. In the Pelvoux massif, the Callovo-Oxfordian sediments are commonly considered to mark the end of the rifting event (Barféty, 1985). According to the thermal model of McKenzie (1978), this post-rift period should correspond to thermal relaxation/cooling in the lithosphere, not heating. It has been noted however that sediment burial in extremely thinned domain can contribute to keeping the margin hot for several tens of millions of years after break-up (Pérez-Gussinyé et al., 2024). These recent models confirm what has been documented previously for example, in the Pyrenees rift, that crustal geothermal gradients can be kept high due to high sedimentation rates during the post-rift phase (e.g., Lescoutre et al., 2019; Vacherat et al., 2014).

In the Western Alps the post-rift phase related to oceanic spreading in the Alpine Tethys is dated at 180–160 Ma. However, as shown by Célini et al. (2023), even though the Early Jurassic syn-rift subsidence was significant in the Vocontian basin, and that contribution of post-rift sediment burial should be accounted for, they were not sufficient taken together to explain the measured temperatures achieved in the Early Cretaceous. A second stage of heating was therefore proposed corresponding to the Early Cretaceous (ca. 100 Ma, Aptian-Albian) phase of rifting that is recorded by mafic rock crystallization at 90 Ma in the Valaisan rift domain (e.g., Liati et al., 2005; Loprieno et al., 2011). We suggest the Early Cretaceous thermal event recorded in the Pelvoux massif reflects a second thinning event on the European paleomargin.

The Mesozoic thermal event recorded in our ZFT data suggests a rise in temperature up to ca. 300°C, which is in agreement with the high temperature (300–350°C) obtained with RSCM by Bellanger et al. (2015) for the Pelvoux Jurassic basins and by Balansa et al. (2022) and Célini et al. (2023) for the Digne Nappe and the Remollon Dome, which are part of the Vocontian basin (Figures 7 and 8). We propose that the Pelvoux massif was buried below sedimentary successions on the European paleomargin until the late Early Cretaceous, which coupled with

10.1029/2024TC008498

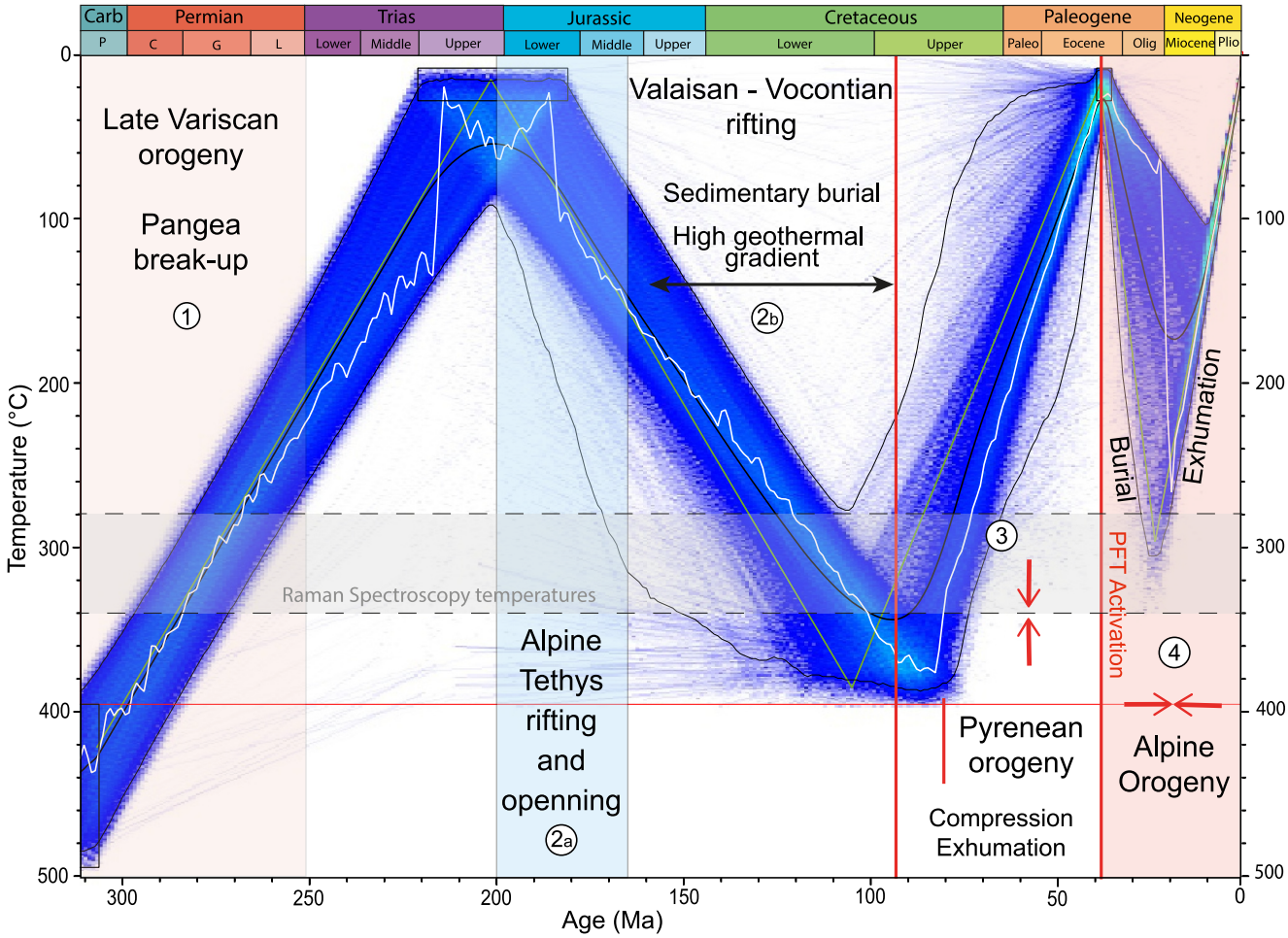

Figure 7. Tectonic interpretation to the time—temperature history of the Pelvoux massif based on block 2 thermal evolution. The numerals 1, 2a, 2b, 3, and 4 are used to identify each phase set out in the conclusion.

a high geothermal gradient, allowed the thermal peak recorded by RSCM analysis to be reached (Figures 7 and 9a). Average geothermal gradients observed for extended crusts are on the order of 50–75°C/km (Kolawole & Evenick, 2023). A sedimentary burial of 4–7 km is therefore required during the Jurassic to the late Early Cretaceous to reproduce the temperatures reached in our models. This estimate is consistent with the preserved thickness of 3–5 km for the Jurassic and Cretaceous strata (Debrand-Passard et al., 1984).

The Mesozoic heating phase ends with rapid cooling to surface temperatures before deposition of the Priabonian trilogy, including the Nummilitic limestone, Globigerina marls and Champsaur flysch (Féraud et al., 1995; Mulder et al., 2010) (Figure 7). The pre-Priabonian exhumation, most likely Late Cretaceous in age, conforms with compressional deformation of the Mesozoic cover and basement that is documented in the southern part of the Pelvoux massif (Dumont et al., 2008, 2012; Ford, 1996; Lazarre, 1997). This exhumation agrees with the D1 shortening phase associated with the Pyrenean deformation described in the Western Alps (Ceriani & Schmid, 2004; Dumont et al., 2008, 2022) and in the Provence (e.g., Bilau, Bienveignant, et al., 2023; Bilau, Rolland, et al., 2023). It is further consistent with the beginning of the fall in relative sea level and lower sediment accumulation contemporaneous to folding in the Vocontian basin (e.g., Cairanne et al., 2002; Ford & Stahel, 1995; Grosheny et la., 2017; Schreiber et al., 2011), which might have occurred during the Turonian-Coniacian as indicated by the angular unconformity in the Devoluy massif (Debelmas, 1989; Glangeaud & d'Albissin, 1958). Our results indicate that the north-south shortening was widespread in SE France over a distance of about 200 km from the Provence to the Pelvoux massif during the Late Cretaceous period (Figure 9b), which is also supported by the greater crustal thickness in the Pelvoux massif than in other ECMs to the north

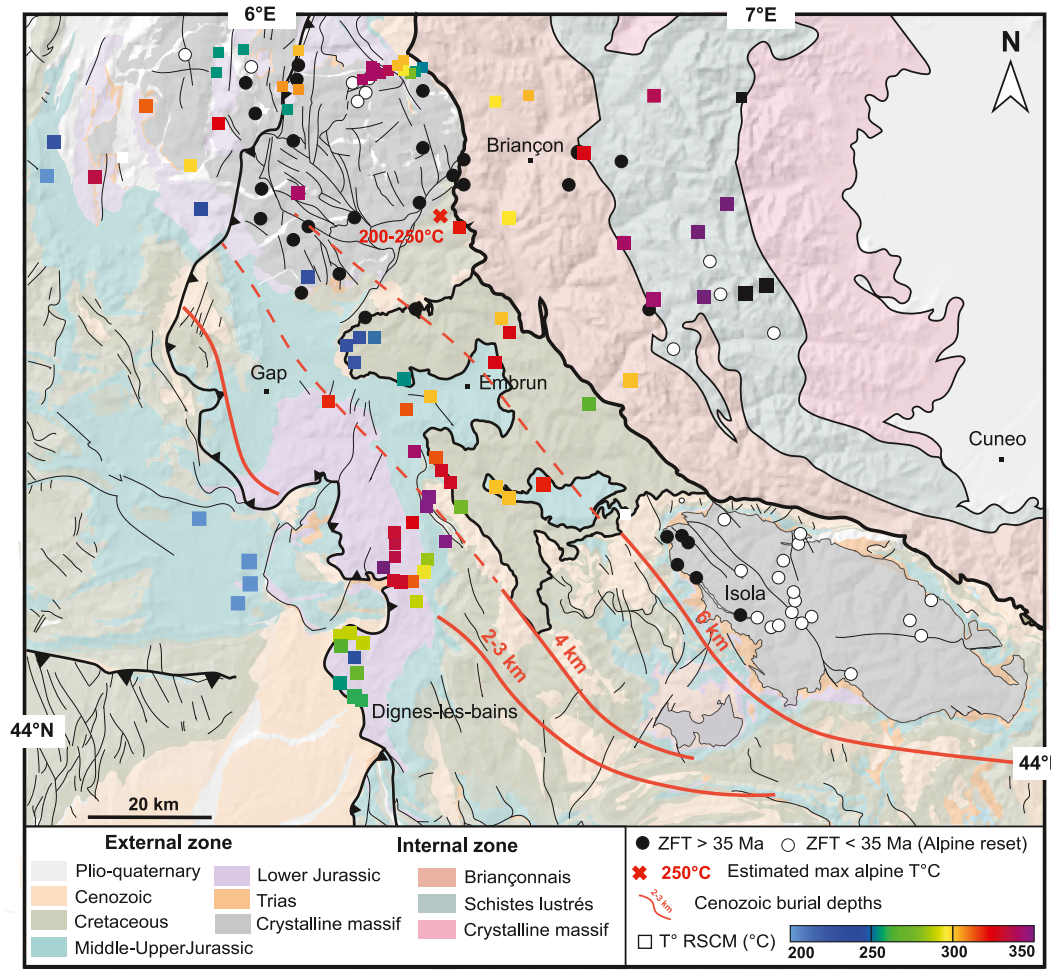

Figure 8. Thermal constraints in the southwestern Alps from RSCM (Balansa et al., 2022; Bellanger et al., 2015; Célini et al., 2023), ZFT reset/unreset ages from this study and Seward et al. (1999), Bigot-Cormier et al. (2000), van der Beek et al. (2010), and Girault et al. (2022) and burial depths inferred from AFT (Jourdan et al., 2013; Labaume et al., 2008; Schwartz et al., 2007).

(Schwartz et al., 2024). Because the Mesozoic heating period is better preserved into the south of the Pelvoux massif, it can be suggested that the structure of the Pelvoux massif inherited from rifting/necking processes was more pronounced in the south than in the north of the massif. The question then arises as to whether this Late Cretaceous shortening from 110 to 70 Ma is linked to the Pyrenean collision *sensu stricto* that is thought to have started after the Turonian-Coniacian between Iberia-Ebro and Europe (Angrand & Mouthereau, 2021), or to the convergence between Europe and Adria, which initiated at around 110 Ma (e.g., Handy et al., 2010). The paleogeographic reconstruction at 80 Ma (Figure 9b), reveals that Ebro-Iberia, Adria and Europe could have been in contact at this period. The distributed deformation associated with the onset of collision between the micro-plates renders the definition of a plate boundary obsolete in this complex region. The Late Cretaceous "Pyrenean" deformation could well mark the onset of an "Eo-Alpine" collision between Adria and Europe in the southern Alps. Further studies will be needed to address this issue.

5.2.2. Post-Priabonian "Alpine" Thermal Evolution

Our inverse models define a heating period starting at 30–25 Ma, with maximal temperatures reaching 200–300°C depending on the blocks (Figure 5). Block 1 shows the highest temperature of 300°C acquired in the Pelvoux massif during the Alpine event at 35–25 Ma. Such temperature should lead to the full annealing of the fission tracks in zircon. However, thermal modeling from this block predicts partial annealing of the ZFT ages of 131.5 and 94.8 Ma (see also Figure S5 in Supporting Information S1). The considerable variability in temperature

10.1029/2024TC008498

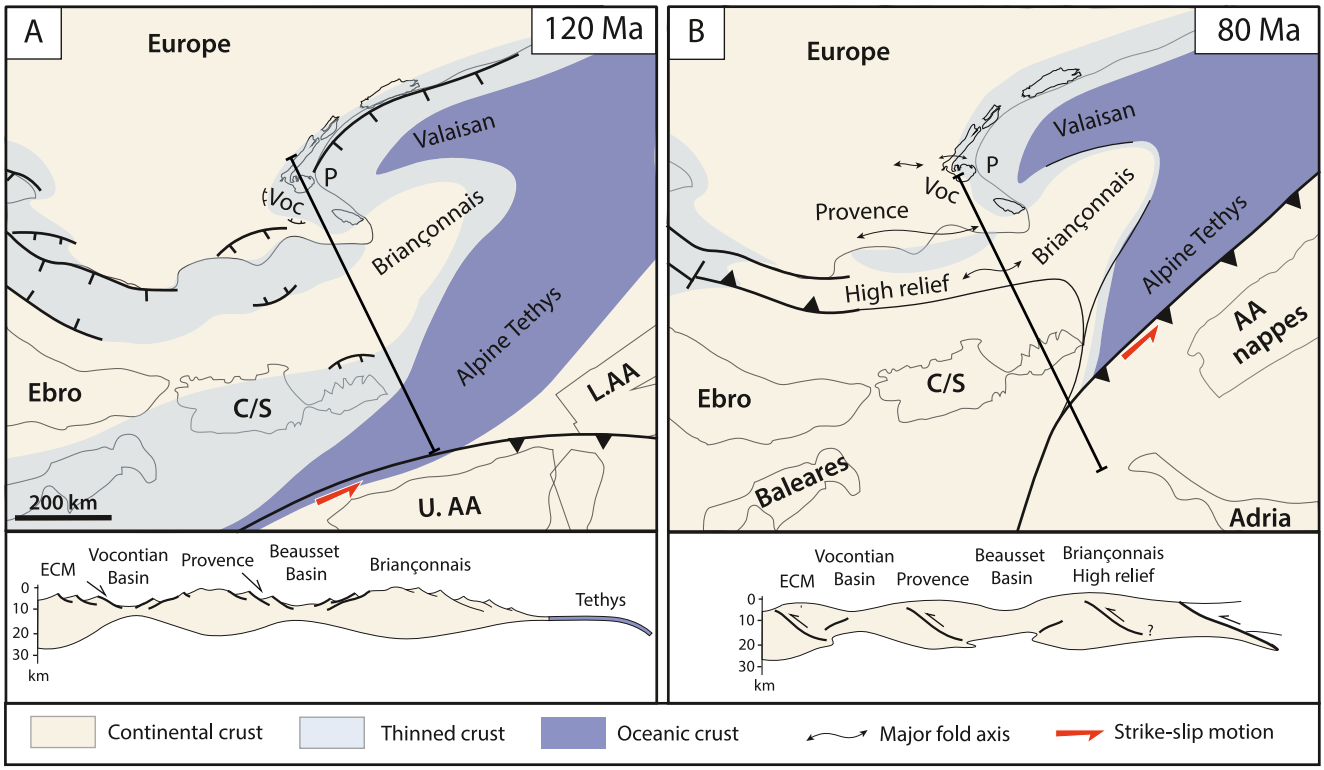

Figure 9. : Kinematic and paleogeographic reconstruction of Ebro/Corsica-Sardinia block and Adria relative to Europe in the Early and Late Cretaceous. (a) at 120 Ma, opening of Valaisan basin and Pyrenean rift. (b) at 80 Ma, tectonic inversion which led to the early stage Pelvoux exhumation. P: Pelvoux; C/S: Corsica/Sardinia; L.AA: Lower Austro-Alpine nappe; U. AA: Upper Austro-Alpine nappe; Voc: Vocontian Basin. Position of tectonic blocks modified after van Hinsbergen et al. (2020); Angrand and Mouthereau (2021); Le Breton et al. (2021).

estimates between the Max likelihood model and the Max posterior model at 100 Ma suggests that our data do not permit to choose between the two possibilities (annealing or not) (Figure 5a). This lack of resolution can be attributed to the absence of apatite track length data for these samples. However, the maximum predicted temperature agrees with published RSCM data, indicating that temperature of approximatively 330°C have been reached in the northern part of the Pelvoux massif (Bellanger et al., 2015) (Figure 8). This is also in accordance with thermos-paleomagnetic data from the Emparis and Bourg d'Oisans basins (blocks 1 and 4), that indicate cooling from temperatures as high as 335°C after 24 Ma (Crouzet et al., 1999, 2001; Ménard & Rochette, 1992). These temperatures have been previously interpreted as related to the Alpine tectonic burial for the entire massif beneath Penninic units (Bellanger et al., 2015). However, new low-temperature thermochronological data and thermal models show that the maximum post-Priabonian "Alpine" temperature are significantly lower in the southern part of the Pelvoux massif. They are of 200 and 180°C in blocks 2 and 3, respectively, and of 220°C toward the east in blocks 5 and 6, closer to the PFT (Figure 5). These temperatures are consistent with previous studies that estimated a maximum peak temperature of 250°C, corresponding to blocks 5 and 6, beneath the PFT (Figure 8) (Potel & Trullenque, 2012; Seward et al., 1999; Tricart et al., 2007). These authors also indicated that burial temperature toward the southwest of the Pelvoux massif, in the region corresponding to block 2 and 3, were close to 180°C. This estimate agrees with a 6 km burial under tectonic nappes and/or Priabonian to Oligo-Miocene sedimentary deposits estimated to the south of the Pelvoux massif and at the border of the Argentera massif (Labaume et al., 2008) (Figure 8). The temperature difference of 40–70°C between block 2 and block 6 appears to be controlled by the distance relative to the PFT, as the burial heating increases close to PFT (Figure 3b). It can also be argued that within block 6, the temperature and burial were greater toward the north in agreement with previous estimates of burial temperatures in the northern ECMs by Bellanger et al. (2015), who however only considered tectonic and not sedimentary burial. This degree of Alpine heating can also explain the complex pattern of Mesozoic heating based on the partially reset ZFT ages. This partial reset, which resulted in younger apparent cooling ages, is more significant toward the east and the north due to the increasing burial of the

Pelvoux massif, which results in less well constrained time/temperature models in these parts of the massif, as observed for blocks 5 and 6 and the total annealing of ZFT ages of block 1 (Figures 6d and 6e).

6. Conclusion

This study highlights the potential of multi-method thermochronology to unravel the complex polyphase tectonic and thermal histories of a low-grade metamorphic terrain. Our analyses in the Pelvoux massif, which lies at the intersection of the Alpine and Pyrenean-Provence orogens, reveal the succession of four main tectono-thermal events (Figure 7):

1. The first one is related to differential exhumation between 340 and 300 Ma during the late Variscan metamorphic event associated with crustal-scale vertical strike slip fault activity, leading to the anastomosed East Variscan shear zone.
2. The following Mesozoic heating event reflects Early Jurassic and Early Cretaceous rifting episodes related to the opening of the Alpine Tethys (a) and Valaisan/Vocontian domains (b), respectively. Temperatures up to 350°C were reached in the Pelvoux massif at the end of the Early Cretaceous as a result of continuous crustal thinning and depositional burial (Figure 9a).
3. Cooling and exhumation that occurred from the Late Cretaceous to the Priabonian were contemporaneous with north-south Pyrenean-Provence shortening, in a context of rift inversion. This deformation could be a far-field effect of onset of an "Eo-Alpine" collision between Adria and Europe (Figure 9b).
4. The Pelvoux massif then recorded heating during the Oligocene (35–25 Ma) caused by deposition of the Late Eocene to Oligocene Flysch in the Alpine foreland, and underthrusting beneath the PFT in the eastern part of the massif. This heating event was unevenly recorded in the massif. In the north, the Mesozoic rift-related event was overprinted by Alpine collision-related temperatures of more than 300°C, while it was preserved to the south due to temperatures of maximum 250°C during Alpine burial.

Conflict of Interest

The authors declare no conflicts of interest relevant to this study.

Data Availability Statement

The data is available at https://doi.org/10.18709/PERSCIDO.2024.07.DS410 (Boschetti, 2024). A ReadMe.txt file describing the content of the two files is available with them (Boschetti, 2024).

Acknowledgments
This study was made possible thanks to ministerial funding from the SDU2E doctoral school at Paul Sabatier III University and by additional the funding by the RFG-Alps programme, coordinated by the BRGM. We would also like to thank Kerry Gallagher for his advice and guidance on QTQt models and ZFT processing in our case. We also thank also Kelly Thomson and the second anonymous reviewer for their constructive remarks.

References

Angrand, P., & Mouthereau, F. (2021). Evolution of the Alpine orogenic belts in the Western Mediterranean region as resolved by the kinematics of the Europe-Africa diffuse plate boundary. *BSGF-Earth Sciences Bulletin*, *192*(1), 42. https://doi.org/10.1051/bsgf/2021031

Balansa, J., Espurt, N., Hippolyte, J. C., Philip, J., & Caritg, S. (2022). Structural evolution of the superimposed Provençal and Subalpine fold-thrust belts (SE France). *Earth-Science Reviews*, *227*, 103972. https://doi.org/10.1016/j.earscirev.2022.103972

Ballevre, M., Manzotti, P., & Dal Piaz, G. V. (2018). Pre-alpine (Variscan) inheritance: A key for the location of the future Valaisan Basin (Western Alps). *Tectonics*, *37*(3), 786–817. https://doi.org/10.1002/2017TC004633

Barféty, J. C. (1985). Le Jurassique dauphinois entre Durance et Rhône: étude stratigraphique et géodynamique; évolution d'une portion de la marge nord téthysienne (Alpes occidentales françaises) (Doctoral dissertation, Université Scientifique et Médicale de Grenoble).

Barféty, J. C., & Gidon, M. (1983). La stratigraphie et la structure de la couverture dauphinoise au Sud de Bourg d'Oisans. Leurs relations avec les déformations synsédimentaires jurassiques. *Geologie Alpine*, *59*, 5–32.

Barféty, J. C., Gidon, M., & Mouterde, R. (1970). Observations stratigraphiques et structurales sur le Mézozoïque des environs de Bourg-d'Oisans (Isère). *Geologie Alpine*, *46*, 23–28.

Bellahsen, N., Mouthereau, F., Boutoux, A., Bellanger, M., Lacombe, O., Jolivet, L., & Rolland, Y. (2014). Collision kinematics in the western external Alps. *Tectonics*, *33*(6), 1055–1088. https://doi.org/10.1002/2013TC003453

Bellanger, M., Augier, R., Bellahsen, N., Jolivet, L., Monié, P., Baudin, T., & Beyssac, O. (2015). Shortening of the European Dauphinois margin (Oisans Massif, Western Alps): New insights from RSCM maximum temperature estimates and 40Ar/39Ar in situ dating. *Journal of Geodynamics*, *83*, 37–64. https://doi.org/10.1016/j.jog.2014.09.004

Beltrando, M., Manatschal, G., Mohn, G., Dal Piaz, G. V., Brovarone, A. V., & Masini, E. (2014). Recognizing remnants of magma-poor rifted margins in high-pressure orogenic belts: The Alpine case study. *Earth-Science Reviews*, *131*, 88–115. https://doi.org/10.1016/j.earscirev.2014.01.001

Beucher, R., van der Beek, P., Braun, J., & Batt, G. E. (2012). Exhumation and relief development in the Pelvoux and Dora-Maira massifs (Western Alps) assessed by spectral analysis and inversion of thermochronological age transects. *Journal of Geophysical Research*, *117*(F3), F03030. https://doi.org/10.1029/2011JF002240

Bigot-Cormier, F., Poupeau, G., & Sosson, M. (2000). Dénudations différentielles du massif cristallin externe alpin de l'Argentera (Sud-Est de la France) révélées par thermochronologie traces de fission (apatites, zircons). *Comptes Rendus de l'Academie des Sciences - Series IIA: Earth and Planetary Science*, *330*(5), 363–370. https://doi.org/10.1016/S1251-8050(00)00127-0

Bigot-Cormier, F., Sosson, M., Poupeau, G., Stéphan, J. F., & Labrin, E. (2006). The denudation history of the Argentera Alpine External Crystalline Massif (Western Alps, France-Italy): An overview from the analysis of fission tracks in apatites and zircons. *Geodinamica Acta*, *19*(6), 455–473. https://doi.org/10.3166/ga.19.455-473

Bilau, A., Bienveignant, D., Rolland, Y., Schwartz, S., Godeau, N., Guihou, A., et al. (2023). The Tertiary structuration of the Western Subalpine foreland deciphered by calcite-filled faults and veins. *Earth-Science Reviews*, *236*, 104270. https://doi.org/10.1016/j.earscirev.2022.104270

Bilau, A., Rolland, Y., Dumont, T., Schwartz, S., Godeau, N., Guihou, A., & Deschamps, P. (2023). Early onset of Pyrenean collision (97–90 Ma) evidenced by U–Pb dating on calcite (Provence, SE France). *Terra Nova*, *35*(5), 413–423. https://doi.org/10.1111/ter.12665

Bilau, A., Rolland, Y., Schwartz, S., Gautheron, C., Dumont, T., Bienveignant, D., et al. (2025). Timing of syn-orogenic extension in the Western Alps revealed by calcite U-Pb and hematite (U-Th)/He dating. *Geoscience Frontiers*, *16*(2), 101969. https://doi.org/10.1016/j.gsf.2024.101969

Bilau, A., Rolland, Y., Schwartz, S., Godeau, N., Guihou, A., Deschamps, P., et al. (2021). Extensional reactivation of the Penninic Frontal Thrust 3 Ma ago as evidenced by U-Pb dating on calcite in fault zone cataclasite. *Solid Earth*, *12*(1), 237–251. https://doi.org/10.5194/se-12-237-2021

Bogdanoff, S., Michard, A., Mansour, M., & Poupeau, G. (2000). Apatite fission track analysis in the Argentera massif: Evidence of contrasting denudation rates in the external crystalline massifs of the western Alps. *Terra Nova*, *12*(3), 117–125. https://doi.org/10.1046/j.13653121.2000.123281.x

Boschetti, L. (2024). Thermochronology of the Pelvoux massif [Dataset]. *PerSCiDO*. https://doi.org/10.18709/PERSCIDO.2024.07.DS410

Boschetti, L., Schwartz, S., Rolland, Y., Dumont, T., & Nouibat, A. (2023). A new tomographic-petrological model for the Ligurian-Provence back-arc basin (North-Western Mediterranean Sea). *Tectonophysics*, *868*, 230111. https://doi.org/10.1016/j.tecto.2023.230111

Brandon, M. T., Roden-Tice, M. K., & Garver, J. I. (1998). Late Cenozoic exhumation of the Cascadia accretionary wedge in the Olympic Mountains, northwest Washington State. *Geological Society of America Bulletin*, *110*(8), 985–1009. https://doi.org/10.1130/00167606(1998)110<0985:LCEOTC>2.3.CO;2

Brunsmann, Q. (2023). L'arc des Alpes occidentales: cinématique et mécanismes de formation au jour de nouvelles données structurales et paléomagnétiques (Doctoral dissertation, Sorbonne Université). Retrieved from https://theses.hal.science/tel-04480313v1

Cairanne, G., Aubourg, C., & Pozzi, J. P. (2002). Syn-folding remagnetization and the significance of the small circle test: Examples from the Vocontian trough (SE France). *Physics and Chemistry of the Earth, Parts A/B/C*, *27*(25–31), 1151–1159. https://doi.org/10.1016/S1474-7065(02)00106-7

Carosi, R., D'Addario, E., Mammoliti, E., Montomoli, C., & Simonetti, M. (2016). Geology of the northwestern portion of the Ferriere-Mollieres Shear Zone, Argentera Massif, Italy. *Journal of Maps*, *12*(sup1), 466–475. https://doi.org/10.1080/17445647.2016.1243491

Carosi, R., Montomoli, C., Tiepolo, M., & Frassi, C. (2012). Geochronological constraints on post- collisional shear zones in the Variscides of Sardinia (Italy). *Terra Nova*, *24*(1), 42–51. https://doi.org/10.1111/j.1365-3121.2011.01035.x

Célini, N., Pichat, A., Mouthereau, F., Ringenbach, J. C., & Callot, J. P. (2023). Along-strike variations of structural style in the external Western Alps (France): Review, insights from analogue models and the role of salt. *Journal of Structural Geology*, *179*, 105048. https://doi.org/10.1016/j.jsg.2023.105048

Cenki-Tok, B., Darling, J. R., Rolland, Y., Dhuime, B., & Storey, C. D. (2014). Direct dating of mid-crustal shear zones with synkinematic allanite: New in situ U-Th-Pb geochronological approaches applied to the Mont Blanc massif. *Terra Nova*, *26*(1), 29–37. https://doi.org/10.1111/ter.12066

Ceriani, S., Fügenschuh, B., & Schmid, S. M. (2001). Multi-stage thrusting at the "Penninic Front" in the Western Alps between Mont Blanc and Pelvoux massifs. *International Journal of Earth Sciences*, *90*(3), 685–702. https://doi.org/10.1007/s005310000188

Ceriani, S., & Schmid, S. M. (2004). From NS collision to WNW-directed post-collisional thrusting and folding: Structural study of the Frontal Penninic Units in Savoie (western Alps, France). *Eclogae Geologicae Helvetiae*, *97*(3), 347–369. https://doi.org/10.1007/s00015-004-1129-2

Cogné, N., Chew, D. M., Donelick, R. A., & Ansberque, C. (2020). LA-ICP-MS apatite fission track dating: A practical zeta-based approach. *Chemical Geology*, *531*, 119302. https://doi.org/10.1016/j.chemgeo.2019.119302

Cogné, N., Derycke, A., & Gallagher, K. (2024). The McClure mountain syenite apatite as a potential age control reference material for LA-ICP-MS AFT and U-Pb double dating. *Geostandards and Geoanalytical Research*, *48*(2), 381–391. https://doi.org/10.1111/ggr.12545

Corsini, M., & Rolland, Y. (2009). Late evolution of the southern European Variscan belt: Exhumation of the lower crust in a context of oblique convergence. *Comptes Rendus Geoscience*, *341*(23), 214–223. https://doi.org/10.1016/j.crte.2008.12.002

Crouzet, C., Ménard, G., & Rochette, P. (1999). High-precision three-dimensional paleothermometry derived from paleomagnetic data in an Alpine metamorphic unit. *Geology*, *27*(6), 503–506. https://doi.org/10.1130/0091-7613(1999)027<0503:HPTDPD>2.3.CO;2

Crouzet, C., Ménard, G., & Rochette, P. (2001). Cooling history of the Dauphinoise Zone (western Alps, France) deduced from the thermopaleomagnetic record: Geodynamic implications. *Tectonophysics*, *340*(1–2), 79–93. https://doi.org/10.1016/S0040-1951(01)00142-1

Debelmas, J. (1989). One some key features of the evolution of the western Alps. In *Tectonic evolution of the Tethyan region* (pp. 23–42).

Debrand-Passard, S. (Ed.) (1984)., *Synthèse géologique du Sud-Est de la France*, *Editions BRGM* (Vol. 1).

Donelick, R. A., O'Sullivan, P. B., & Ketcham, R. A. (2005). Apatite fission-track analysis. *Reviews in Mineralogy and Geochemistry*, *58*(1), 49–94. https://doi.org/10.2138/rmg.2005.58.3

Dumitru, T. A. (1993). A new computer-automated microscope stage system for fission-track analysis. *Nuclear Tracks and Radiation Measurements*, *21*(4), 575–580. https://doi.org/10.1016/13590189(93)90198-I

Dumont, T., Champagnac, J. D., Crouzet, C., & Rochat, P. (2008). Multistage shortening in the Dauphiné zone (French Alps): The record of alpine collision and implications for pre-alpine restoration. *Swiss Journal of Geosciences*, *101*(S1), 89–110. https://doi.org/10.1007/s00015-0081280-2

Dumont, T., Schwartz, S., Guillot, S., Malusa, M., Jouvent, M., Monié, P., & Verly, A. (2022). Cross-propagation of the western Alpine orogen from early to late deformation stages: Evidence from the Internal Zones and implications for restoration. *Earth-Science Reviews*, *232*, 104106. https://doi.org/10.1016/j.earscirev.2022.104106

Dumont, T., Schwartz, S., Guillot, S., Simon-Labric, T., Tricart, P., & Jourdan, S. (2012). Structural and sedimentary records of the Oligocene revolution in the Western Alpine arc. *Journal of Geodynamics*, *56*, 18–38. https://doi.org/10.1016/j.jog.2011.11.006

Edel, J. B., Schulmann, K., Lexa, O., & Lardeaux, J. M. (2018). Late Palaeozoic palaeomagnetic and tectonic constraints for amalgamation of Pangea supercontinent in the European Variscan belt. *Earth-Science Reviews*, *177*, 589–612. https://doi.org/10.1016/j.earscirev.2017.12.007

Féraud, G., Ruffet, G., Stéphan, J. F., Lapierre, H., Delgado, E., & Popoff, M. (1995). Nouvelles données géochronologiques sur le volcanisme paléogène des Alpes occidentales: Existence d'un événement magmatique bref généralisé. In *Séance Spéciale de la Société géologique de France et de " l'Association des Géologues du SE "Magmatismes dans le sud-est de la France"* (pp. 25–26).

Ford, M. (1996). Kinematics and geometry of early Alpine, basement-involved folds, SW Pelvoux Massif, SE France. *Eclogae Geologicae Helvetiae*, *89*(1), 269–295. https://doi.org/10.5169/seals-167902

Ford, M., & Lickorish, W. H. (2004). Foreland basin evolution around the western Alpine Arc. *Geological Society, London, Special Publications*, *221*(1), 39–63. https://doi.org/10.1144/GSL.SP.2004.221.01.04

Ford, M., & Stahel, U. (1995). The geometry of a deformed carbonate slope-basin transition: The Ventoux-Lure fault zone, SE France. *Tectonics*, *14*(6), 1393–1410. https://doi.org/10.1029/95tc02522

Fréville, K., Trap, P., Vanardois, J., Melleton, J., Faure, M., Bruguier, O., et al. (2022). Carboniferous-Permian tectono-metamorphic evolution of the Pelvoux massif (external crystalline massif, western Alps), with discussion on flow kinematics of the Eastern-Variscan shear zone. *Bulletin de la Societe Geologique de France*, *193*(1), 13. https://doi.org/10.1051/bsgf/2022008

Fugenschuh, B., & Schmid, S. M. (2003). Late stages of deformation and exhumation of an orogen constrained by fission-track data: A case study in the western Alps. *Geological Society of America Bulletin*, *115*(11), 1425–1440. https://doi.org/10.1130/B25092.1

Galbraith, R. F. (1990). The radial plot: Graphical assessment of spread in ages. International journal of radiation applications and instrumentation. Part D. *Nuclear Tracks and Radiation Measurements*, *17*(3), 207–214. https://doi.org/10.2307/135563

Galbraith, R. F. (2005). *Statistics for fission track analysis* (p. 219). Chapman & Hall.

Galbraith, R. F., & Laslett, G. M. (1993). Statistical models for mixed fission track ages. *Nuclear Tracks and Radiation Measurements*, *21*(4), 459–470. https://doi.org/10.1016/1359-0189(93)90185-C

Gallagher, K. (2012). Transdimensional inverse thermal history modeling for quantitative thermochronology. *Journal of Geophysical Research*, *117*(B2). https://doi.org/10.1029/2011JB008825

Gallagher, K., Brown, R., & Johnson, C. (1998). Fission track analysis and its applications to geological problems. *Annual Review of Earth and Planetary Sciences*, *26*(1), 519–572. https://doi.org/10.1146/annurev.earth.26.1.519

Gasquet, D., Bertrand, J. M., Paquette, J. L., Lehmann, J., Ratzov, G., de Ascencao Guedes, R., et al. (2010). Miocene to Messinian deformation and hydrothermal activity in a preAlpine basement massif of the French western Alps: New U-Th-Pb and argon ages from the Lauzière massif. *Bulletin de la Societe Geologique de France*, *181*(3), 227–241. https://doi.org/10.2113/gssgfbull.181.3.227

Giacomini, F., Dallai, L., Carminati, E., Tiepolo, M., & Ghezzo, C. (2008). Exhumation of a Variscan orogenic complex: Insights into the composite granulitic–amphibolitic metamorphic basement of south-east Corsica (France). *Journal of Metamorphic Geology*, *26*(4), 403–436. https://doi.org/10.1111/j.1525-1314.2008.00768.x

Girault, J. B., Bellahsen, N., Bernet, M., Pik, R., Loget, N., Lasseur, E., et al. (2022). Exhumation of the Western Alpine collisional wedge: New thermochronological data. *Tectonophysics*, *822*, 229155. https://doi.org/10.1016/j.tecto.2021.229155

Glangeaud, L., & d'Albissin, M. (1958). Les phases tectoniques du NE du Dévoluy et leur influence structurologique. *Bulletin de la Societe Geologique de France*, *6*(7), 675–688.

Gleadow, A., Harrison, M., Kohn, B., Lugo-Zazueta, R., & Phillips, D. (2015). The fish Canyon Tuff: A new look at an old low-temperature thermochronology standard. *Earth and Planetary Science Letters*, *424*, 95–108. https://doi.org/10.1016/j.epsl.2015.05.003

Glotzbach, C., Reinecker, J., Danišík, M., Rahn, M., Frisch, W., & Spiegel, C. (2008). Neogene exhumation history of the Mont Blanc massif, western Alps. *Tectonics*, *27*(4). https://doi.org/10.1029/2008TC002257

Gremmel, J., Duclaux, G., Corsini, M., & Bascou, J. (2023). Constrictional flow and strain partitioning during oblique deformation: Insights from the Variscan Tanneron massif, SE France. *Tektonika*, *2*, 112–140.

Grosheny, D., Ferry, S., Lécuyer, C., Thomas, A., & Desmares, D. (2017). The Cenomanian–Turonian Boundary Event (CTBE) on the southern slope of the Subalpine Basin (SE France) and its bearing on a probable tectonic pulse on a larger scale. *Cretaceous Research*, *72*, 39–65. https://doi.org/10.1016/j.cretres.2016.11.009

Guillot, S., di Paola, S., Ménot, R. P., Ledru, P., Spalla, M. I., Gosso, G., & Schwartz, S. (2009). Suture zones and importance of strike-slip faulting for Variscan geodynamic reconstructions of the External Crystalline Massifs of the western Alps. *Bulletin de la Societe Geologique de France*, *180*(6), 483–500. https://doi.org/10.2113/gssgfbull.180.6.483

Handy, M. R., Schmid, S. M., Bousquet, R., Kissling, E., & Bernoulli, D. (2010). Reconciling plate-tectonic reconstructions of Alpine Tethys with the geological–geophysical record of spreading and subduction in the Alps. *Earth-Science Reviews*, *102*(3–4), 121–158. https://doi.org/10.1016/j.earscirev.2010.06.002

Hurford, A. J., & Green, P. F. (1983). The zeta age calibration of fission-track dating. *Chemical Geology*, *41*, 285–317. https://doi.org/10.1016/S0009-2541(83)80026-6

Jacob, J. B., Janots, E., Guillot, S., Rubatto, D., Fréville, K., Melleton, J., & Faure, M. (2022). HT overprint of HP granulites in the Oisans–Pelvoux Massif: Implications for the dynamics of the Variscan collision in the external Western Alps. *Lithos*, *416*, 106650. https://doi.org/10.1016/j.lithos.2022.106650

Jammes, S., & Huismans, R. S. (2012). Structural styles of mountain building: Controls of lithospheric rheologic stratification and extensional inheritance. *Journal of Geophysical Research*, *117*(B10), B10403. https://doi.org/10.1029/2012JB009376

Jochum, K. P., Weis, U., Stoll, B., Kuzmin, D., Yang, Q., Raczek, I., et al. (2011). Determination of reference values for NIST SRM 610–617 glasses following ISO guidelines. *Geostandards and Geoanalytical Research*, *35*(4), 397–429. https://doi.org/10.1111/j.1751-908X.2011.00120.x

Jourdon, A., Le Pourhiet, L., Mouthereau, F., & Masini, E. (2019). Role of rift maturity on the architecture and shortening distribution in mountain belts. *Earth and Planetary Science Letters*, *512*, 89–99. https://doi.org/10.1016/j.epsl.2019.01.057

Ketcham, R. A., Carter, A., Donelick, R. A., Barbarand, J., & Hurford, A. J. (2007). Improved modeling of fission-track annealing in apatite. *American Mineralogist*, *92*(5–6), 799–810. https://doi.org/10.2138/am.2007.2281

Kirkland, C. L., Yakymchuk, C., Szilas, K., Evans, N., Hollis, J., McDonald, B., & Gardiner, N. J. (2018). Apatite: A U-Pb thermochronometer or geochronometer? *Lithos*, *318*, 143–157. https://doi.org/10.1016/j.lithos.2018.08.007

Kolawole, F., & Evenick, J. C. (2023). Global distribution of geothermal gradients in sedimentary basin. *Geoscience Frontiers*, *14*(6), 101685. https://doi.org/10.1016/j.gsf.2023.101685

Labaume, P., Jolivet, M., Souquière, F., & Chauvet, A. (2008). Tectonic control on diagenesis in a foreland basin: Combined petrologic and thermochronologic approaches in the Grès d'Annot basin (Late Eocene–early Oligocene, French–Italian external Alps). *Terra Nova*, *20*(2), 95–101. https://doi.org/10.1111/j.1365-3121.2008.00793.x

Lagabrielle, Y., Brovarone, A. V., & Ildefonse, B. (2015). Fossil oceanic core complexes recognized in the blueschist metaophiolites of Western Alps and Corsica. *Earth-Science Reviews*, *141*, 1–26. https://doi.org/10.1016/j.earscirev.2014.11.004

Lanari, P., Rolland, Y., Schwartz, S., Vidal, O., Guillot, S., Tricart, P., & Dumont, T. (2014). P–T–t estimation of deformation in low-grade quartz-feldspar-bearing rocks using thermodynamic modelling and 40Ar/39Ar dating techniques: Example of the Plan-de-Phasy shear zone unit (Briançonnais Zone, Western Alps). *Terra Nova*, *26*(2), 130–138. https://doi.org/10.1111/ter.12079

Laurent, J. C. (1992). Les épisodes magmatiques filoniens basiques du Massif des Ecrins-Pelvoux entre Carbonifère et Lias (Doctoral dissertation, Université Joseph-Fourier-Grenoble I). tel-00509743.

Lazarre, J. (1997). Modélisation 3D de l'interface socle varisque-couverture alpine dans le Massif du Pelvoux (Hautes Alpes, France) -Tectonique des socles et bassins à la limite secondairetertiaire (Doctoral dissertation, Université Claude Bernard-Lyon I). tel-00614882.

Leloup, P. H., Arnaud, N., Sobel, E. R., & Lacassin, R. (2005). Alpine thermal and structural evolution of the highest external crystalline massif: The Mont Blanc. *Tectonics*, *24*(4). https://doi.org/10.1029/2004TC001676

Lemoine, M., Bas, T., Arnaud-Vanneau, A., Arnaud, H., Dumont, T., Gidon, M., et al. (1986). The continental margin of the Mesozoic Tethys in the western Alps. *Marine and Petroleum Geology*, *3*(3), 179–199. https://doi.org/10.1016/0264-8172(86)90044-9

Lescoutre, R., Tugend, J., Brune, S., Masini, E., & Manatschal, G. (2019). Thermal evolution of asymmetric hyperextended magma-poor rift systems: Results from numerical modeling and Pyrenean field observations. *Geochemistry, Geophysics, Geosystems*, *20*(10), 4567–4587. https://doi.org/10.1029/2019GC008600

Liati, A., Froitzheim, N., & Fanning, C. M. (2005). Jurassic ophiolites within the Valais domain of the western and central Alps: Geochronological evidence for re-rifting of oceanic crust. *Contributions to Mineralogy and Petrology*, *149*(4), 446–461. https://doi.org/10.1007/s00410-005-0658-7

Loprieno, A., Bousquet, R., Bucher, S., Ceriani, S., Dalla Torre, F. H., Fügenschuh, B., & Schmid, S. M. (2011). The Valais units in Savoy (France): A key area for understanding the palaeogeography and the tectonic evolution of the western Alps. *International Journal of Earth Sciences*, *100*(5), 963–992. https://doi.org/10.1007/s00531-010-0595-1

Ludwig, K. R. (1980). Calculation of uncertainties of U-Pb isotope data. *Earth and Planetary Science Letters*, *46*(2), 212–220. https://doi.org/10.1016/0012-821X(80)90007-2

Mai Yung Sen, V., Rolland, Y., Valla, P. G., Jaillet, S., Bruguier, O., Bienveignant, D., & Robert, X. (2025). Fold-and-Thrust belt and early alpine relief recorded by calcite U–Pb dating of an uplifted Paleo-Canyon (Vercors Massif, France). *Terra Nova*. https://doi.org/10.1111/ter.12761

Manatschal, G., Chenin, P., Lescoutre, R., Miró, J., Cadenas, P., Saspiturry, N., et al. (2021). The role of inheritance in forming rifts and rifted margins and building collisional orogens: A Biscay-Pyrenean perspective. *BSGF-Earth Sciences Bulletin*, *192*(1), 55. https://doi.org/10.1051/bsgf/2021042

Masini, E., Manatschal, G., Mohn, G., & Unternehr, P. (2012). Anatomy and tectono-sedimentary evolution of a rift-related detachment system: The example of the Err detachment (central Alps, SE Switzerland). *Geological Society of America Bulletin*, *124*(9–10), 1535–1551. https://doi.org/10.1130/B30557.1

McDowell, F. W., McIntosh, W. C., & Farley, K. A. (2005). A precise ^{40}Ar–^{39}Ar reference age for the Durango apatite (U–Th)/He and fission-track dating standard. *Chemical Geology*, *214*(3–4), 249–263. https://doi.org/10.1016/j.chemgeo.2004.10.002

McIntosh, K., van Avendonk, H., Lavier, L., Lester, W. R., Eakin, D., Wu, F., et al. (2013). Inversion of a hyper-extended rifted margin in the southern Central Range of Taiwan. *Geology*, *41*(8), 871–874. https://doi.org/10.1130/G34402.1

McKenzie, D. (1978). Some remarks on the development of sedimentary basins. *Earth and Planetary Science Letters*, *40*(1), 25–32. https://doi.org/10.1016/0012-821X(78)90071-7

Menard, G., & Rochette, P. (1992). Utilisation de reaimantations postmetamorphiques pour une etude de l'evolution tectonique et thermique tardive dans les Alpes occidentales (France). *Bulletin de la Societe Geologique de France*, *163*(4), 381–392.

Mercier, A., Leloup, P. H., Courrioux, G., Caritg, S., Lopez, S., Grandjean, P., et al. (2023). Large thrusting and late faulting shape the Aiguilles Rouges crystalline massif (Western Alps), structural implications. *Tectonophysics*, *847*, 229691. https://doi.org/10.1016/j.tecto.2022.229691

Mesalles, L., Mouthereau, F., Bernet, M., Chang, C. P., Lin, A. T. S., Fillon, C., & Sengelen, X. (2014). From submarine continental accretion to arc-continent orogenic evolution: The thermal record in southern Taiwan. *Geology*, *42*(10), 907–910. https://doi.org/10.1130/G35854.1

Mohn, G., Manatschal, G., Beltrando, M., & Haupert, I. (2014). The role of rift-inherited hyper- extension in Alpine-type orogens. *Terra Nova*, *26*(5), 347–353. https://doi.org/10.1111/ter.12104

Mohn, G., Manatschal, G., Beltrando, M., Masini, E., & Kusznir, N. (2012). Necking of continental crust in magma-poor rifted margins: Evidence from the fossil Alpine Tethys margins. *Tectonics*, *31*(1), TC1012. https://doi.org/10.1029/2011TC002961

Morillon, A. C., Féraud, G., Sosson, M., Ruffet, G., Crevola, G., & Lerouge, G. (2000). Diachronous cooling on both sides of a major strike slip fault in the Variscan Maures Massif (south-east France), as deduced from a detailed ^{40}Ar/^{39}Ar study. *Tectonophysics*, *321*(1), 103–126. https://doi.org/10.1016/S0040-1951(00)00076-7

Mouthereau, F., Angrand, P., Jourdon, A., Ternois, S., Fillon, C., Calassou, S., et al. (2021). Cenozoic mountain building and topographic evolution in western Europe: Impact of billions of years of lithosphere evolution and plate kinematics. *BSGF-Earth Sciences Bulletin*, *192*(1), 56. https://doi.org/10.1051/bsgf/2021040

Mouthereau, F., Filleaudeau, P. Y., Vacherat, A., Pik, R., Lacombe, O., Fellin, M. G., et al. (2014). Placing limits to shortening evolution in the Pyrenees: Role of margin architecture and implications for the Iberia/Europe convergence. *Tectonics*, *33*(12), 2283–2314. https://doi.org/10.1002/2014TC003663

Mouthereau, F., Watts, A. B., & Burov, E. (2013). Structure of orogenic belts controlled by lithosphere age. *Nature Geoscience*, *6*(9), 785–789. https://doi.org/10.1038/ngeo1902

Mulder, T., Callec, Y., Parize, O., Joseph, P., Schneider, J. L., Robin, C., et al. (2010). High-resolution analysis of submarine lobes deposits: Seismic-scale outcrops of the Lauzanier area (SE Alps, France). *Sedimentary Geology*, *229*(3), 160–191. https://doi.org/10.1016/j.sedgeo.2009.11.005

Naeser, C. W., Zimmermann, R. A., & Cebula, G. T. (1981). Fission-track dating of apatite and zircon: An interlaboratory comparison. *Nuclear Tracks*, *5*(1–2), 65–72. https://doi.org/10.1016/0191-278X(81)90027-5

Pérez-Gussinyé, M., Xin, Y., Cunha, T., Ram, R., Andrés-Martínez, M., Dong, D., & García-Pintado, J. (2024). Synrift and post-rift thermal evolution of rifted margins: A re-evaluation of classic models of extension. *Geological Society, London, Special Publications*, *547*(1), SP547–2023. https://doi.org/10.1144/SP547-2023-128

Potel, S., & Trullenque, G. (2012). Very low-grade metamorphism in the para-autochthonous sedimentary cover of the Pelvoux massif (Western Alps, France). *Swiss Journal of Geosciences*, *105*(2), 235–247. https://doi.org/10.1007/s00015-012-0102-8

Rahn, M. K., Brandon, M. T., Batt, G. E., & Garver, J. I. (2004). A zero-damage model for fission-track annealing in zircon. *American Mineralogist*, *89*(4), 473–484. https://doi.org/10.2138/am-20040401

Reiners, P. W., & Brandon, M. T. (2006). Using thermochronology to understand orogenic erosion. *Annual Review of Earth and Planetary Sciences*, *34*(1), 419–466. https://doi.org/10.1146/annurev.earth.34.031405.125202

Ribes, C., Manatschal, G., Ghienne, J. F., Karner, G. D., Johnson, C. A., Figueredo, P. H., et al. (2019). The syn-rift stratigraphic record across a fossil hyper-extended rifted margin: The example of the northwestern Adriatic margin exposed in the Central Alps. *International Journal of Earth Sciences*, *108*(6), 2071–2095. https://doi.org/10.1007/s00531-019-01750-6

Rolland, Y., Corsini, M., & Demoux, A. (2009). Metamorphic and structural evolution of the Maures- Tanneron massif (SE Variscan chain): Evidence of doming along a transpressional margin. *Bulletin de la Societe Geologique de France*, *180*(3), 217–230. https://doi.org/10.2113/gssgfbull.180.3.217

Rolland, Y., & Rossi, M. (2016). Two-stage fluid flow and element transfers in shear zones during collision burial-exhumation cycle: Insights from the Mont Blanc Crystalline Massif (Western Alps). *Journal of Geodynamics*, *101*, 88–108. https://doi.org/10.1016/j.jog.2016.03.016

Roux, M., Bourseau, J. P., Bas, T., Dumont, T., de Graciansky, P. C., Lemoine, M., & Rudkiewicz, J. L. (1988). Bathymetric evolution of the Tethyan margin in the western Alps (data from stalked crinoids): A reappraisal of eustatism problems during the Jurassic. *Bulletin de la Societe Geologique de France*, *4*(4), 633–641. https://doi.org/10.2113/gssgfbull.iv.4.633

Rudkiewicz, J. L. (1988). Structure et subsidence de la marge téthysienne entre Grenoble et Briançon au Lias et au Dogger (Doctoral dissertation, Ecole Nationale Supérieure des Mines de Paris). tel-00712814.

Sanchez, G., Rolland, Y., Schneider, J., Corsini, M., Oliot, E., Goncalves, P., et al. (2011). Dating low-temperature deformation by 40Ar/39Ar on white mica, insights from the Argentera-Mercantour Massif (SW Alps). *Lithos*, *125*(1–2), 521–536. https://doi.org/10.1016/j.lithos.2011.03.009

Schmid, S. M., Fügenschuh, B., Kissling, E., & Schuster, R. (2004). Tectonic map and overall architecture of the Alpine orogen. *Eclogae Geologicae Helvetiae*, *97*(1), 93–117. https://doi.org/10.1007/s00015-004-1113-x

Schmid, S. M., Pfiffner, O. A., Froitzheim, N., Schönborn, G., & Kissling, E. (1996). Geophysical- geological transect and tectonic evolution of the Swiss-Italian Alps. *Tectonics*, *15*(5), 1036–1064. https://doi.org/10.1029/96TC00433

Schoene, B., & Bowring, S. A. (2006). U–Pb systematics of the McClure mountain syenite: Thermochronological constraints on the age of the 40Ar/39Ar standard MMhb. *Contributions to Mineralogy and Petrology*, *151*(5), 615–630. https://doi.org/10.1007/s00410-006-0077-

Schreiber, D. X., Giannerini, G., & Lardeaux, J. M. (2011). The Southeast France basin during Late Cretaceous times: The spatiotemporal link between Pyrenean collision and Alpine subduction. *Geodinamica Acta*, *24*(1), 21–35. https://doi.org/10.3166/ga.24.21-35

Schwartz, S., Lardeaux, J. M., Tricart, P., Guillot, S., & Labrin, E. (2007). Diachronous exhumation of HP–LT metamorphic rocks from south-western Alps: Evidence from fission-track analysis. *Terra Nova*, *19*(2), 133–140. https://doi.org/10.1111/j.1365-3121.2006.00728.x

Schwartz, S., Rolland, Y., Nouibat, A., Boschetti, L., Bienveignant, D., Dumont, T., et al. (2024). Role of mantle indentation in collisional deformation evidenced by deep geophysical imaging of Western Alps. *Communications Earth & Environment*, *5*(1), 17. https://doi.org/10.1038/s43247-023-01180-y

Seward, D., Ford, M., Burgisser, J., Lickorish, H., Williams, E. D., & Meckel, L. D. (1999). Preliminary results of fission track analyses in the Southern Pelvoux area, SE France. *Mem. Sci. Geol. Padova*, *51*, 25–31.

Seward, D., & Mancktelow, N. S. (1994). Neogene kinematics of the central and western Alps: Evidence from fission-track dating. *Geology*, *22*(9), 803–806. https://doi.org/10.1130/00917613(1994)022<0803:NKOTCA>2.3.CO;2

Simonetti, M., Carosi, R., Montomoli, C., Corsini, M., Petroccia, A., Cottle, J. M., & Iaccarino, S. (2020). Timing and kinematics of flow in a transpressive dextral shear zone, Maures Massif (Southern France). *International Journal of Earth Sciences*, *109*(7), 2261–2285. https://doi.org/10.1007/s00531-020-01898-6

Simonetti, M., Carosi, R., Montomoli, C., Cottle, J. M., & Law, R. D. (2020). Transpressive deformation in the southern European Variscan belt: New insights from the Aiguilles Rouges massif (western Alps). *Tectonics*, *39*(6), e2020TC006153. https://doi.org/10.1029/2020TC006153

Simonetti, M., Carosi, R., Montomoli, C., Langone, A., D'Addario, E., & Mammoliti, E. (2018). Kinematic and geochronological constraints on shear deformation in the Ferriere-Mollières shear zone (Argentera-Mercantour Massif, Western Alps): Implications for the evolution of the Southern European Variscan Belt. *International Journal of Earth Sciences*, *107*(6), 2163–2189. https://doi.org/10.1007/s00531-018-1593-y

Simonetti, M., Langone, A., Bonazzi, M., Corvò, S., & Maino, M. (2023). Tectono-metamorphic evolution of a post-Variscan mid-crustal shear zone in relation to the Tethyan rifting (Ivrea-Verbano Zone, Southern Alps). *Journal of Structural Geology*, *173*, 104896. https://doi.org/10.1016/j.jsg.2023.104896

Simon-Labric, T., Rolland, Y., Dumont, T., Heymes, T., Authemayou, C., Corsini, M., & Fornari, M. (2009). 40Ar/39Ar dating of Penninic front tectonic displacement (W Alps) during the lower Oligocene (31–34 Ma). *Terra Nova*, *21*(2), 127–136. https://doi.org/10.1111/j.13653121.2009.00865.x

Sue, C., Tricart, P., Dumont, T., & Pêcher, A. (1997). Raccourcissement polyphase dans le massif du Pelvoux (Alpes occidentales): Exemple du chevauchement de socle de Villard-Notre-Dame. *Comptes Rendus de l'Academie des Sciences - Series IIA: Earth and Planetary Science*, *324*(10), 847–854. https://doi.org/10.1016/S1251-8050(97)82520-7

Tagami, T., Galbraith, R. F., Yamada, R., & Laslett, G. M. (1998). Revised annealing kinetics of fission tracks in zircon and geological implications. In *Advances in fission-track geochronology: A selection of papers presented at the international workshop on fission-track dating, Ghent, Belgium, 1996* (pp. 99–112). Springer. https://doi.org/10.1007/978-94-015-91331_8

Thomson, S. N., Gehrels, G. E., Ruiz, J., & Buchwaldt, R. (2012). Routine low-damage apatite U-Pb dating using laser ablation–multicollector–ICPMS. *Geochemistry, Geophysics, Geosystems*, *13*(2). https://doi.org/10.1029/2011GC003928

Tricart, P., Schwartz, S., Sue, C., Poupeau, G., & Lardeaux, J. M. (2001). La denudation tectonique de la zone ultradauphinoise et l'inversion du front brianconnais au sud-est du Pelvoux (Alpes occidentales); une dynamique miocene a actuelle. *Bulletin de la Societe Geologique de France*, *172*(1), 49–58. https://doi.org/10.2113/172.1.49

Tricart, P., Van der Beek, P., Schwartz, S., & Labrin, E. (2007). Diachronous late-stage exhumation across the western Alpine arc: Constraints from apatite fission-track thermochronology between the Pelvoux and Dora-Maira massifs. *Journal of the Geological Society*, *164*(1), 163–174. https://doi.org/10.1144/0016-76492005-174

Vacherat, A., Mouthereau, F., Pik, R., Bernet, M., Gautheron, C., Masini, E., et al. (2014). Thermal imprint of rift-related processes in orogens as recorded in the Pyrenees. *Earth and Planetary Science Letters*, *408*, 296–306. https://doi.org/10.1016/j.epsl.2014.10.014

Vai, G. B. (2003). Development of the palaeogeography of Pangaea from late Carboniferous to early Permian. *Palaeogeography, Palaeoclimatology, Palaeoecology*, *196*(1–2), 125–155. https://doi.org/10.1016/S0031-0182(03)00316-X

van Der Beek, P. A., Valla, P. G., Herman, F., Braun, J., Persano, C., Dobson, K. J., & Labrin, E. (2010). Inversion of thermochronological age–elevation profiles to extract independent estimates of denudation and relief history—II: Application to the French western Alps. *Earth and Planetary Science Letters*, *296*(1–2), 9–22. https://doi.org/10.1016/j.epsl.2010.04.032

van Hinsbergen, D. J., Torsvik, T. H., Schmid, S. M., Maţenco, L. C., Maffione, M., Vissers, R. L., et al. (2020). Orogenic architecture of the Mediterranean region and kinematic reconstruction of its tectonic evolution since the Triassic. *Gondwana Research*, *81*, 79–229. https://doi.org/10.1016/j.gr.2019.07.009

Wiederkehr, M., Sudo, M., Bousquet, R., Berger, A., & Schmid, S. M. (2009). Alpine orogenic evolution from subduction to collisional thermal overprint: The 40Ar/39Ar age constraints from the Valaisan Ocean, central Alps. *Tectonics*, *28*(6). https://doi.org/10.1029/2009TC002496

Yamada, R., Murakami, M., & Tagami, T. (2007). Statistical modelling of annealing kinetics of fission tracks in zircon; Reassessment of laboratory experiments. *Chemical Geology*, *236*(1–2), 75–91. https://doi.org/10.1016/j.chemgeo.2006.09.002

York, D., Evensen, N. M., Martınez, M. L., & De Basabe Delgado, J. (2004). Unified equations for the slope, intercept, and standard errors of the best straight line. *American Journal of Physics*, *72*(3), 367–375. https://doi.org/10.1119/1.1632486